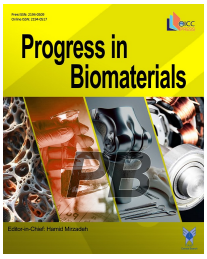

Volume 13, Issue 2, 132405 (1-19)

Progress in Biomaterials (PIBM)

https://doi.org/10.57647/pibm.2024.132405

Controlling Hydroxyapatite Ratio in Poly(glycerol sebacate)/ Polycaprolactone /Chitosan Scaffolds Directs Chondrogenesis of Adipose-Derived Mesenchymal Stem Cells for Cartilage Regeneration

Pardis Yousefi Talouki[1], Reyhaneh Tamimi[2], Shahrokh Shojaei[3,*], Soheila Zamanlui Benisi[3], Saeed Hesami Tackallou[3], Salar Mohammadi Shabestari[4], Mohhamad hossein Nasrolah[3], Vahabodin Goodarzi[5,*]

[1]*Department of Biomedical Engineering, QaS.C., Islamic Azad University, Qaemshahr, Iran.*
[2]*Department of Biomedical Engineering, Amirkabir University of Technology, Tehran, Iran.*
[3]*Department of Biomedical Engineering, CT.C., Islamic Azad University, Tehran, Iran.*
[4]*Department of Polymer, School of Chemical Engineering, College of Engineering, University of Tehran, Tehran, Iran.*
[5]*Tissue Engineering and Regenerative Medicine Research Center, Baqiyatallah University of Medical Sciences, Tehran, Iran.*
[*]**Corresponding authors:** shahrokhshojaei@iau.ir, and v.goodarzi@hotmail.com

© 2024 The Author(s)

Original Research

Abstract:

The limited self-repair capacity of articular cartilage necessitates innovative tissue engineering strategies. This study aimed to develop a tunable, biomimetic scaffold platform by combining poly(glycerol sebacate) (PGS), polycaprolactone (PCL), chitosan (Ch), and nano-hydroxyapatite (nHA). Five scaffold variants-PGS, PGS/PCL, PGS/PCL/Ch, and nHA-loaded composites (3% and 5% w/w)-were fabricated via salt leaching. Several characterization tests have been conducted on the designed scaffolds. Biocompatibility and biofunctionality were assessed with human adipose-derived mesenchymal stem cells (hADSCs) through cell viability assays (MTT), SEM for cell attachment, evaluation of chondrogenic gene expression (COL2A1, ACAN, SOX9), and Alcian Blue staining for glycosaminoglycan (GAG) deposition.

SEM and Elemental Mapping confirmed an irregular, interconnected porous structure and the homogeneous dispersion of nHA within the polymer matrix. FTIR analysis demonstrated successful chemical interactions between the components. The incorporation of nHA significantly enhanced hydrophilicity, compressive strength, and thermal stability (TGA). The swelling test revealed that the PGS/PCL/Ch scaffold had the highest liquid retention capacity, while mechanical tests indicated that the 5% nHA composite exhibited the highest compressive strength and a significantly improved elongation at break compared to the 3% nHA variant. Biological evaluations demonstrated that PGS/PCL/Ch/nHA scaffolds, particularly the 5% variant, supported markedly superior cell viability, attachment, and chondrogenic differentiation.

The collective data confirm the PGS/PCL/Ch/5% nHA scaffold as the optimal candidate, synergizing elastomeric properties, bioactivity, and chondroinductivity for clinical translation.

Keywords:

Poly (glycerol sebacate); Chitosan; Hydroxyapatite nanoparticles; Cartilage tissue engineering; Chondrogenic differentiation; Mesenchymal stem cells

Cite this article: Yousefi Talouki, P., Tamimi, R., Shojaei, S., Zamanlui Benisi, S., Hesami Tackallou, S., Mohammadi Shabestari, S., Nasrolah, M. H., Goodarzi, V. Controlling Hydroxyapatite Ratio in Poly(glycerol sebacate)/ Polycaprolactone /Chitosan Scaffolds Directs Chondrogenesis of Adipose-Derived Mesenchymal Stem Cells for Cartilage Regeneration. *Progress in Biomaterials* **13**(2), Article 05 (2024).

1. Introduction

Articular cartilage (AC) is a specialized connective tissue with limited self-repair capacity due to its avascular, aneural nature and low chondrocyte density (Jelodari et al., 2022; Liu et al., 2021; Tew et al., 2001). This fundamental biological constraint presents three major challenges for effective regeneration: First, the structural-mechanical challenge of replicating the unique biphasic viscoelasticity and load-bearing capacity (elastic modulus: 0.1-2 MPa) of native

cartilage (Balakrishnan and Banerjee, 2011; Silva et al., 2020; Zhao et al., 2021). Second, the biological integration challenge of achieving seamless integration with both underlying subchondral bone and surrounding native cartilage (Dorotka et al., 2005; Shahzadi et al., 2018; Shi et al., 2021; Solheim et al., 2013). Third, the cellular differentiation challenge of reliably directing stem cell differentiation toward stable hyaline cartilage rather than fibrocartilage (Biondi et al., 2008; Mad Jin et al., 2015; Rezk et al., 2020).

Conventional clinical approaches, including microfracture and autologous chondrocyte implantation, face significant limitations in addressing these challenges. Microfracture typically generates biomechanically inferior fibrocartilage, while autologous chondrocyte implantation involves complex, multi-stage procedures with donor site morbidity and inconsistent outcomes (Dorotka et al., 2005; Solheim et al., 2013). These shortcomings have motivated the development of advanced tissue engineering strategies that can more comprehensively address the multifaceted nature of cartilage regeneration.

An ideal tissue engineering scaffold must simultaneously address all three challenges through strategic material design. This has driven interest in hybrid composites that combine natural polymers, synthetic polymers, and bioactive ceramics to create multifunctional platforms (Jelodari et al., 2022; Mad Jin et al., 2015; Zhao et al., 2021). In this context, we developed a tri-component system comprising PGS, PCL, and chitosan, reinforced with nHA, where each component serves a specific purpose in overcoming the fundamental limitations of cartilage regeneration. Therefore, the precise problem this research addresses is the absence of a single scaffold system that can simultaneously overcome these three interconnected challenges, necessitating a multi-material approach where each component strategically addresses a specific limitation.

PGS provides essential elastomeric properties to mimic cartilage's native viscoelasticity but requires reinforcement for load-bearing applications (Rai et al., 2012; Rezk et al., 2020). PCL offers long-term structural integrity but suffers from hydrophobicity that limits cell adhesion (Hu and Nukavarapu, 2019; Zhao et al., 2021). Chitosan addresses this limitation by enhancing wettability, bioactivity, and antibacterial properties (Garcia et al., 2021; Kumar et al., 2019; Neves et al., 2011), though its inherent mechanical weakness necessitates further reinforcement (Ge et al., 2012; Gellynck et al., 2008). The incorporation of nHA serves not merely as a mechanical reinforcement but as an active biological cue that promotes osteochondral integration and directs chondrogenic differentiation (Baji et al., 2006; Eshraghi and Das, 2012; Shahzadi et al., 2018; Shi et al., 2021).

While previous approaches have primarily utilized nHA as a passive reinforcing agent, our systematic investigation of nHA concentration (3-5 wt.%) as a critical tunable parameter represents a paradigm shift toward active, material-driven control of stem cell fate. This approach aligns with emerging trends in biomaterials design, as highlighted by Sharma et al. in their review of advanced dental materials, where they emphasize the importance of "target-specific tuneable mechanics and bioactivity" through "hybrid synergistic approaches" (Sharma et al., 2021).

Furthermore, when compared with specific studies in cartilage tissue engineering, the distinct advantage of our strategy becomes evident. While Huang et al. successfully demonstrated that HAP doping in gelatin scaffolds improves rheological properties and supports chondrogenic differentiation in a pig model, their work treated HAP mainly as a material additive to enhance printability and bioactivity (Huang et al., 2021). Similarly, Talouki et al. focused on nHA-reinforced PGS/PCL/gelatin scaffolds for enhanced chondrogenic differentiation (Talouki et al., 2023), and Shahbazi et al. emphasized mechanical optimization of sodium alginate/nanoclay/HA composites. In contrast to these valuable contributions, our work establishes a quantitative relationship between specific nHA ratios and chondrogenic differentiation of hADSCs within a unique tri-component system, positioning nHA not merely as a bioactive additive but as a central design parameter that actively directs cellular fate. This represents a significant advancement toward the "multi-criteria optimization" called for in modern tissue engineering strategies. In recent years, cartilage tissue engineering has made significant progress, although challenges remain. In the conducted study, PGS/PCL/Gel scaffolds with nanohydroxyapatite (nHA) were evaluated for hADSCs culture, showing desirable properties such as high hydrophilicity, improved mechanical strength, and enhanced degradability (Shojaei et al., 2019). In another study, PCL/-PLA blends with HA nanoparticles were prepared, which increased the crystalline peaks of PCL and showed higher water absorption and creep strain at acidic pH 4, while no significant changes were observed at pH 7 (Talouki et al., 2023). Previous studies have shown that mechanical stimuli, such as shear stress and stretching, influence cell differentiation and the expression of endothelial and smooth muscle genes (Farjaminejad et al., 2021). Combining optimized scaffolds with controlled mechanical stimulation can provide a suitable environment to guide hADSCs differentiation into cartilage cells (Shoajei et al., 2014).

The present study hypothesizes that precise control of nHA concentration in PGS/PCL/chitosan scaffolds can actively direct hADSC chondrogenic differentiation without exogenous growth factors. The specific aims were to: (1) fabricate and characterize five scaffold variants with varying nHA content (3%, and 5%); (2) evaluate their physicochemical properties and degradation behavior; (3) assess hADSC viability, proliferation, and chondrogenic differentiation. The novelty of this work lies in establishing nHA concentration as a critical tunable parameter that quantitatively controls chondrogenic outcome in a tri-component scaffold system, representing a significant advancement beyond using nHA as merely a passive reinforcing agent.

2. Materials and methods

2.1 Materials

All chemicals were used as received without further purification. Sebacic acid (Sigma-Aldrich, USA, $>$ 98%) and glycerol (Sigma-Aldrich, USA, $>$ 99%) were used for PGS synthesis. Poly(ε-caprolactone) (PCL, Sigma-

Aldrich, USA, Mw $\sim$ 80,000 g/mol), medium molecular weight chitosan (190-310 kDa, degree of deacetylation: 85%, Sigma-Aldrich), hydroxyapatite nanoparticles (nHA, $<$ 100 nm, Sigma-Aldrich, $\geq$ 97%), chloroform (Sigma-Aldrich, USA, $>$ 99%), isopropanol (Sigma-Aldrich, USA, $\geq$ 99.5%), hexamethylene diisocyanate (HDI, Merck, Germany, $\geq$ 99%), phosphate-buffered saline (PBS, pH 7.3, Gibco), MTT (3-(4,5-dimethylthiazol-2-yl)-2,5-diphenyltetrazolium bromide, Carl Roth, Germany), dimethyl sulfoxide (DMSO, Sigma-Aldrich, $\geq$ 99.9%), sodium chloride (NaCl, Sigma-Aldrich, $\geq$ 99%), fetal bovine serum (FBS, Gibco), ethylenediaminetetraacetic acid (EDTA, Merck, Germany, $\geq$ 99%), and glutaraldehyde (Sigma-Aldrich, 25% solution in water) were used as received. Human adipose-derived mesenchymal stem cells (hADSCs) were procured from Stem Cell Technology Research Center (Iran).

2.2 Scaffold fabrication

2.2.1 Synthesis protocol

PGS Prepolymer. Sebacic acid and glycerol (1:1 molar ratio) were polycondensed at 120 °C for 30 min under nitrogen, followed by vacuum curing (24 h, 120 °C) (Rostamian et al., 2020; Talouki et al., 2023).

PGS/PCL/Ch Blend. PGS and PCL were dissolved in DMSO (24 h, room temperature) (Talouki et al., 2023). Chitosan was dissolved in 10% acetic acid and mixed with the PGS/PCL solution. Tin octanoate catalyst (0.1 wt.%) and HDI (crosslinker, 1:1.2 NCO:OH ratio) were added under stirring (30 min).

Porogen Leaching. The mixture was cast into molds with NaCl particles (200-300 µm), dried (24 h, RT), and leached in distilled water (7 days) to create pores.

nHA Incorporation. For nHA-loaded scaffolds, nanoparticles were dispersed in chloroform/ Dimethyl Formamide (DMF) (1:1) via sonication (15 min) before blending (Talouki et al., 2023) (Total solvent volume: 10 mL).

2.3 Scaffold characterization

2.3.1 Microstructural characterization

The morphological features of PGS/PCL/Ch/HA scaffolds containing 3% and 5% HA nanoparticles were analyzed using scanning electron microscopy (SEM, TESCAN MIRA III). Samples were sputter-coated with a 10 nm gold layer prior to imaging to evaluate pore architecture, nanoparticle dispersion, and surface topography.

2.3.2 Elemental composition analysis

Elemental mapping was performed using energy-dispersive X-ray spectroscopy (EDX) coupled with SEM (TESCAN MIRA II equipped with SAMX detector, acceleration voltage: 20 kV). This technique enabled identification and spatial distribution analysis of calcium (Ca), phosphorus (P), and oxygen (O) within the hydroxyapatite nanoparticles, providing verification of nanoparticle incorporation and dispersion homogeneity throughout the scaffold matrix.

2.3.3 Crystalline structure evaluation

X-ray diffraction (XRD) patterns were recorded using a Philips PW1730 instrument (Cu-Kα, $\lambda = 1.5406$ Å) in $\theta - 2\theta$ configuration. Scaffold crystallinity was assessed through 2θ scans from 10° to 40° at a step size of 0.02° and scan rate of 1 °/min, with crystalline phases identified by comparison to JCPDS reference patterns (Epp, 2016).

2.3.4 Chemical composition analysis

Fourier-transform infrared spectroscopy (FTIR, Thermo Nicolet AVATAR, USA) was employed to characterize the chemical bonds and functional groups present in both raw materials and composite scaffolds. FTIR measurements were performed in transmission mode covering the 400-4000 cm^{-1} range (resolution: 4 cm^{-1}; 32 scans averaged per spectrum) to ensure adequate signal-to-noise characteristics.

2.3.5 Thermal stability assessment

The thermal decomposition behavior was studied via thermogravimetric analysis (TGA Q600, TA Instruments, USA) with a heating rate of 10 °C/min under N_2 flow. Samples ($\sim$ 10 mg) were heated from 25 °C to 600 °C under nitrogen purge (50 mL/min) at a constant heating rate of 20 °C/min. Weight loss profiles were recorded and analyzed to determine decomposition onset temperatures and residual mass percentages.

2.3.6 Swelling capacity assessment

The hydrophilic properties of the scaffolds were quantified through swelling ratio measurements. Specimens were immersed in phosphate-buffered saline (PBS, pH 7.4) and maintained at 37 °C for 24 h. The PBS absorption percentage was determined using the following equation: (Rezaei et al., 2021).

$$\text{Swelling rate}(\%) = \frac{W_s - W_0}{W_0} \times 100 \quad (1)$$

Table 1. Composition of fabricated scaffolds (wt.%).

Sample	PGS	PCL	Chitosan	HA
PGS	100	0	0	0
PGS/PCL	60	40	0	0
PGS/PCL/Ch	60	20	20	0
PGS/PCL/Ch/3% nHA	60	20	20	3
PGS/PCL/Ch/5% nHA	60	20	20	5

where W_0 denotes the initial dry weight of the scaffolds, while W_s represents the weight after swelling equilibrium.

2.3.7 Surface wettability analysis

The hydrophilic/hydrophobic properties of all scaffold formulations were characterized through static water contact angle measurements using a contact angle goniometer (CAG-20 SE, JIKAN). For each measurement, a 5 µL deionized water droplet was deposited onto the scaffold surface, and the contact angle was recorded after a 20-second equilibration period at ambient temperature (25 °C). Three measurements were taken per sample at different locations to ensure representative results.

2.3.8 *In vitro* degradation profile

The degradation kinetics of the scaffolds (10 × 10 × 15 mm^3) were evaluated by monitoring mass loss in phosphate-buffered saline (PBS, pH 7.4) at 37 °C, over a 40-day period. After recording the initial dry weight (W_0), samples were immersed in PBS and removed at predetermined time intervals (1, 3, 7, 14, 28, and 40 days). The retrieved scaffolds were rinsed with deionized water, dried under vacuum at 37 °C for 24 h, and weighed (W_t) to determine the percentage mass loss according to the equation (Asgharnejad-Laskoukalayeh et al., 2022).

$$\text{Degradation}(\%) = \frac{W_0 - W_t}{W_0} \times 100 \qquad (2)$$

2.3.9 Mechanical characterization

The compressive properties of the scaffolds were evaluated using rectangular specimens (11 × 9 × 9 mm^3) prepared with a precision blade. Uniaxial compression testing was conducted at ambient temperature (25 °C) using a universal testing machine (STM-20, SANTAM, Korea) with a crosshead speed of 2 mm/min until 80% strain was achieved (Talouki et al., 2023). Three replicates were tested for each scaffold formulation to ensure statistical reliability.

2.4 Cellular characterization and biological evaluation

2.4.1 Scaffold preparation and cell culture

Scaffolds were precision-cut to match 96-well plate dimensions (8 mm diameter × 2 mm thickness) and preconditioned overnight in complete medium (α-MEM + 10% FBS) at 37 °C with 5% CO_2 to enhance cell adhesion. hADSCs were harvested from T25 flasks via trypsinization (0.25% Trypsin-EDTA, 3-5 min incubation), neutralized with complete medium, and centrifuged (300 × g, 5 min). Cell counts were determined using a hemocytometer, and 10,000 cells in 10 µL suspension were seeded per scaffold, followed by addition of 90 µL medium. Constructs were cultured for 1, 7, and 14 days for viability assessment.

2.4.2 Cell-scaffold interaction analysis

Morphological Assessment. After 3 days of incubation, cellular adhesion characteristics and spreading behavior were examined by scanning electron microscopy (SEM, TESCAN MIRA III). Samples were fixed in 2.5% glutaraldehyde, dehydrated in ethanol series, and critical-point dried prior to imaging. **Viability Assay**. The cellular metabolic activity on scaffolds was quantitatively evaluated using the MTT (3-(4,5-dimethylthiazol-2-yl)-2,5-diphenyltetrazolium bromide) assay at 24-h, 7-day, and 14-day time points. This colorimetric assay measures mitochondrial dehydrogenase activity in viable cells through the enzymatic conversion of the yellow MTT tetrazolium salt to insoluble purple formazan crystals. For the assay, a 5 mg/mL MTT working solution was first prepared by dissolving 10 mg MTT powder in 2 mL of sterile phosphate-buffered saline (PBS, pH 7.4), followed by filtration through a 0.22 µm membrane. MTT assays were initiated by adding 100 µL of 10% MTT solution to each well containing cell-laden scaffolds (n = 5/group), followed by 4 h incubation (37 °C, 5% CO_2). Following incubation, the medium was carefully aspirated and the insoluble formazan crystals were solubilized by adding 100 µL of dimethyl sulfoxide (DMSO) to each well with gentle agitation for 5 minutes. The formazan product was quantified spectrophotometrically (570 nm measurement, 630 nm reference) using a BioTek Synergy HT system. Cell viability was calculated as a percentage relative to control wells containing cells cultured on standard tissue culture plastic surfaces, with higher absorbance values indicating greater metabolic activity and cell viability. This standardized protocol allowed for reliable comparison of cellular responses across different scaffold compositions and culture durations.

2.4.3 Chondrogenic differentiation evaluation

2.4.3.1. Glycosaminoglycan Deposition

The deposition of cartilage-specific glycosaminoglycans (GAGs) was evaluated using Alcian Blue 8GX staining according to established protocols (Aleksander-Konert et al., 2016). with the following detailed procedure: Scaffold specimens (1 × 1 cm^2) from five experimental groups were prepared in triplicate and seeded with human mesenchymal stem cells at 5×10^5 cells/cm^2. Following 21 days of chondrogenic culture, constructs were fixed with 4% paraformaldehyde for 20 minutes and rinsed with PBS. Samples were stained with 0.1% Alcian Blue 8GX (Sigma-Aldrich) in 0.1N HCl (pH 2.5, prepared by diluting 8.3 mL of 37% HCl in 1L distilled water and adjusting pH with NaOH) for 30 minutes. After washing with distilled water, constructs were counterstained with 0.1% Nuclear Fast Red solution (prepared by dissolving 0.1 g Nuclear Fast Red and 5 g aluminum sulfate in 100 mL distilled water) for 5 minutes. Stained specimens were imaged using an Olympus BX51 microscope. GAG deposition was semi-quantitatively analyzed using a four-point scoring system (0: no staining to 4: intense staining) by two independent blinded observers.

2.4.3.2. Gene Expression Analysis by Quantitative Real-Time PCR

Following 21 days of chondrogenic culture, total RNA was isolated from cell-seeded scaffolds using TRIzol reagent (Kiasist, Iran) according to the manufacturer's protocol. RNA concentration and purity were assessed spectrophotometrically (NanoDrop ND-2000), ensuring an A260/A280 ratio between 1.8 and 2.0. Reverse transcription was performed to synthesize complementary DNA (cDNA) using an Easy cDNA Synthesis Kit (Parstous, Iran). The expres-

sion of chondrogenic differentiation markers-collagen type II (COL2A1), aggrecan (ACAN), and SRY-box transcription factor 9 (SOX9)-was quantified via real-time quantitative PCR (qRT-PCR) using an ABI StepOnePlus thermocycler (Applied Biosystems, USA). The sequence of primers (Sinaclon, Iran) that we used in real-time PCR was as Table 2. Gene expression analysis was conducted using a one-step SYBR Green-based qPCR approach with SYBR Green Master Mix (2X concentration, high ROX, Addbio, Korea). Amplification was performed with 5 min initial denaturation (95 °C), followed by 40 cycles consisting of 15 sec denaturation (95 °C), 15-20 sec annealing (60 °C), and 30 sec extension (72 °C). To ensure data reliability and reproducibility, all reactions were performed in triplicate for each biological sample, with appropriate negative controls included in each run. Relative gene expression levels were calculated using the $2^{\wedge}(-\Delta\Delta)Ct)$ method, with glyceraldehyde-3-phosphate dehydrogenase (GAPDH) serving as the endogenous reference gene for normalization (Zhang et al., 2017).

2.5 Statistical analysis

All experiments were performed with three replicates. Statistical analyses were performed using Statistical Package for the Social Sciences (IBM SPSS Statistics, USA) software. *P*-value < 0.05 was considered statistically significant.

3. Results

3.1 Scaffold characterization

3.1.1 Morphological and structural observations

The scaffolds were prepared using the salt leaching method. The SEM images of PGS/PCL, PGS/PCL/Ch, and PGS/PCL/Ch/HA scaffolds with different nanoparticle concentrations (3% and 5%) are presented in figure 1(a-d). The analysis showed that the scaffolds had an irregular, porous structure with interconnected pores. figure 1(b) demonstrates the uniform morphology of PGS/PCL/Ch, attributed to the favorable chemical interaction between the amine groups in chitosan and the polar functional groups of the sample (Talouki et al., 2023). These chemical interactions are schematically illustrated in figure 2, which provides a visual representation of the hydrogen bonding, ionic interactions, and other molecular-level forces between the scaffold components. The presence of n-HA is more clearly resolved within the yellow squares in figure 1(c, d). The HA nanoparticles were evenly dispersed within the polymer matrix and exhibited strong adhesion, suggesting an effective fabrication approach. This uniform distribution of n-HA is facilitated by surface adhesion and ionic interactions between Ca^{2+} ions, hydroxyl groups in n-HA, and the hydroxyl and amine groups in the PGS/PCL/Ch composite (Horkay and Basser, 2020; Zhang et al., 2017).

Additionally, elemental mapping analysis confirmed the homogeneous distribution of calcium (Ca), phosphorus (P), and oxygen (O), which are the primary components of HA nanoparticles. As shown in Fig. 3 A and B, the atomic percentages of Ca, P, and O increased with the rise in hydroxyapatite content from 3% to 5% in the PGS/PCL/Ch/HA5% scaffold (Asgharnejad-Laskoukalayeh et al., 2022). Higher n-HA concentrations led to improved dispersion, as evidenced by the increased density of colored points in the mapping images, which can be attributed to enhanced electrostatic and hydrogen bonding interactions (Asgharnejad-Laskoukalayeh et al., 2022).

The EDS spectrum further corroborated the elemental composition, showing distinct peaks for Ca, P, and O. The Ca/P atomic ratio, calculated from the EDS counts, was found to be approximately 7.9 for the HA3% scaffold and 2.5 for the HA5% scaffold, indicating a notable change in the calcium phosphate stoichiometry with increasing n-HA content (Table 3).

3.1.2 Hydrophilicity analysis

The hydrophilicity of the scaffolds was evaluated through contact angle measurements. Figure 3 A presents the average contact angle values recorded 30 seconds after water droplet deposition on the scaffold surfaces (Horkay and Basser, 2020; Sani et al., 2021; Zhang et al., 2017). A comprehensive statistical analysis was performed using one-way ANOVA with Tukey's post-hoc test to compare all sample groups, with $p < 0.05$ considered statistically significant. The results demonstrated significant differences among all groups ($p < 0.05$), indicating that compositional modifications substantially affect surface wettability.

Research by Asgharianjad et al. demonstrated that incorporating n-HA into the PGSC/CS composite enhanced scaffold hydrophilicity, which was attributed to the polar surface groups present in n-HA. This incorporation consequently led to a reduction in contact angle measurements (Asgharnejad-Laskoukalayeh et al., 2022).

As illustrated in Fig. 4 A, scaffolds containing both hydroxyapatite and PGS exhibited the highest degree of hydrophilicity, primarily due to their abundant hydroxyl groups. Statistical comparisons revealed that these scaffolds showed significantly lower contact angles compared to

Table 2. Primer sequences for RT-PCR.

Primer name	Forward sequence	Reverse sequence
ACAN	CCTCACCATCCCCTGCTAT	GGGTAGTTGGGCAGTGAGACC
COL2A1	ACCAGGACCAAAGGGACAGAA	GGGCACCTTTTTCACCTTTGT
SOX9	AGAAGGAGAGCGAGGAGGACA	CTTGACGTGCGGCTTGTTCTT
GAPDH	CTTTGGTATCGTGGAAGGAC	GCAGGGATGATGTTCTGG

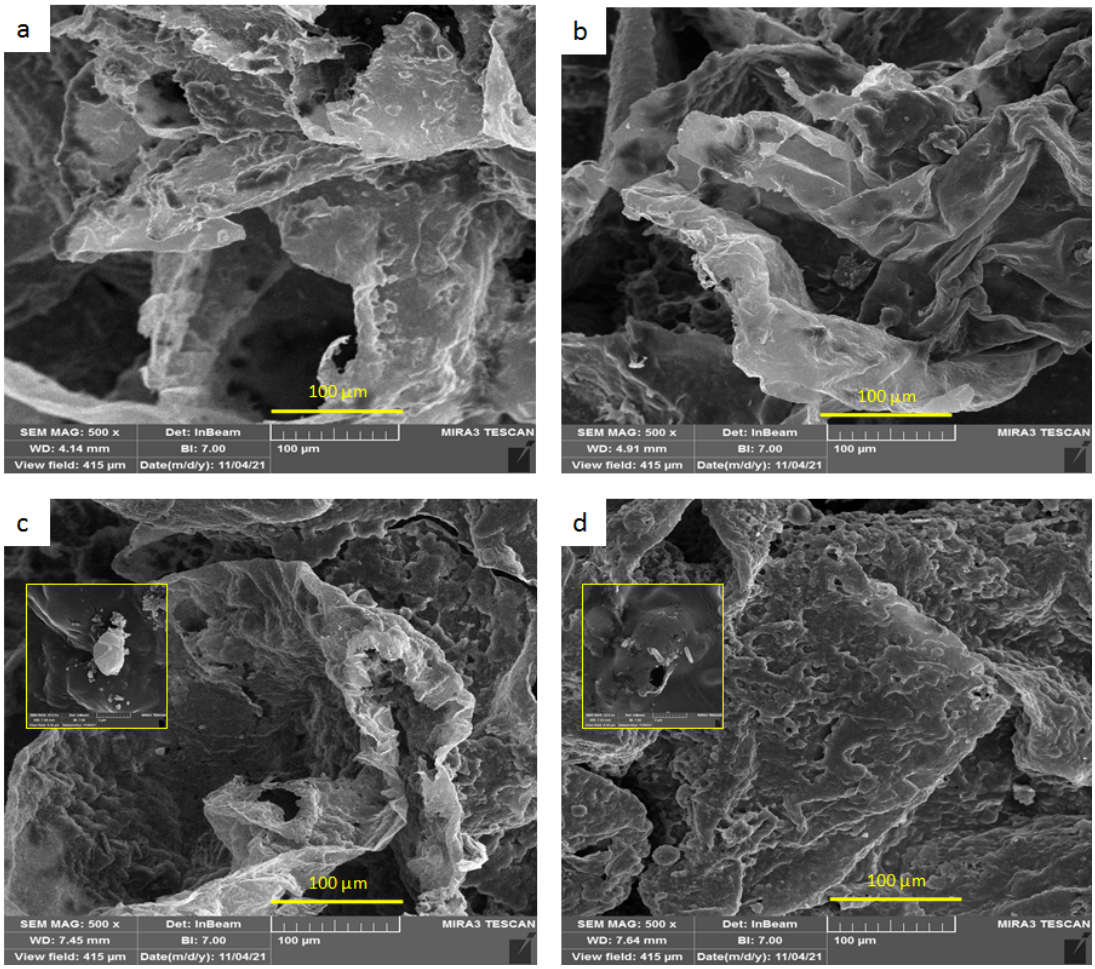

Figure 1. SEM images of (a) PGS/PCL, (b) PGS/PCL/Ch, (c) PGS/PCL/Ch/HA3%, and (d) PGS/PCL/Ch/HA5%.

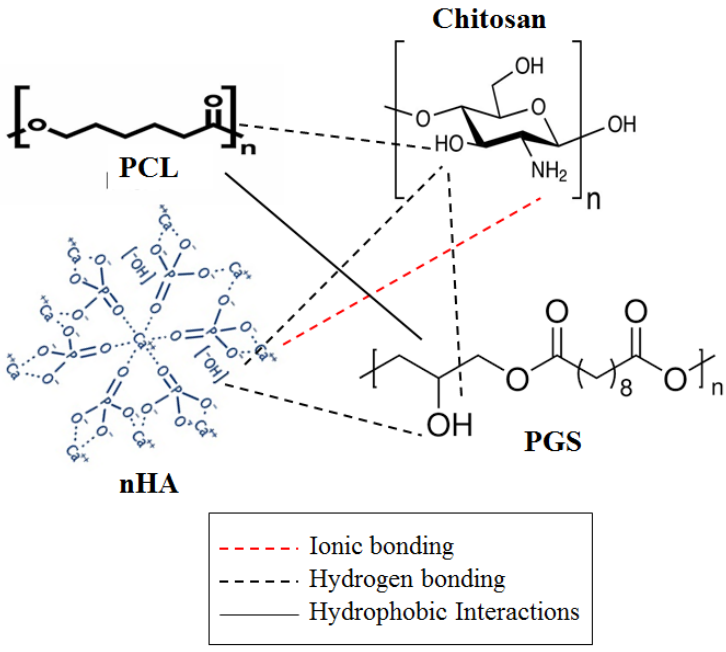

Figure 2. Schematic illustration of chemical interactions between scaffold components.

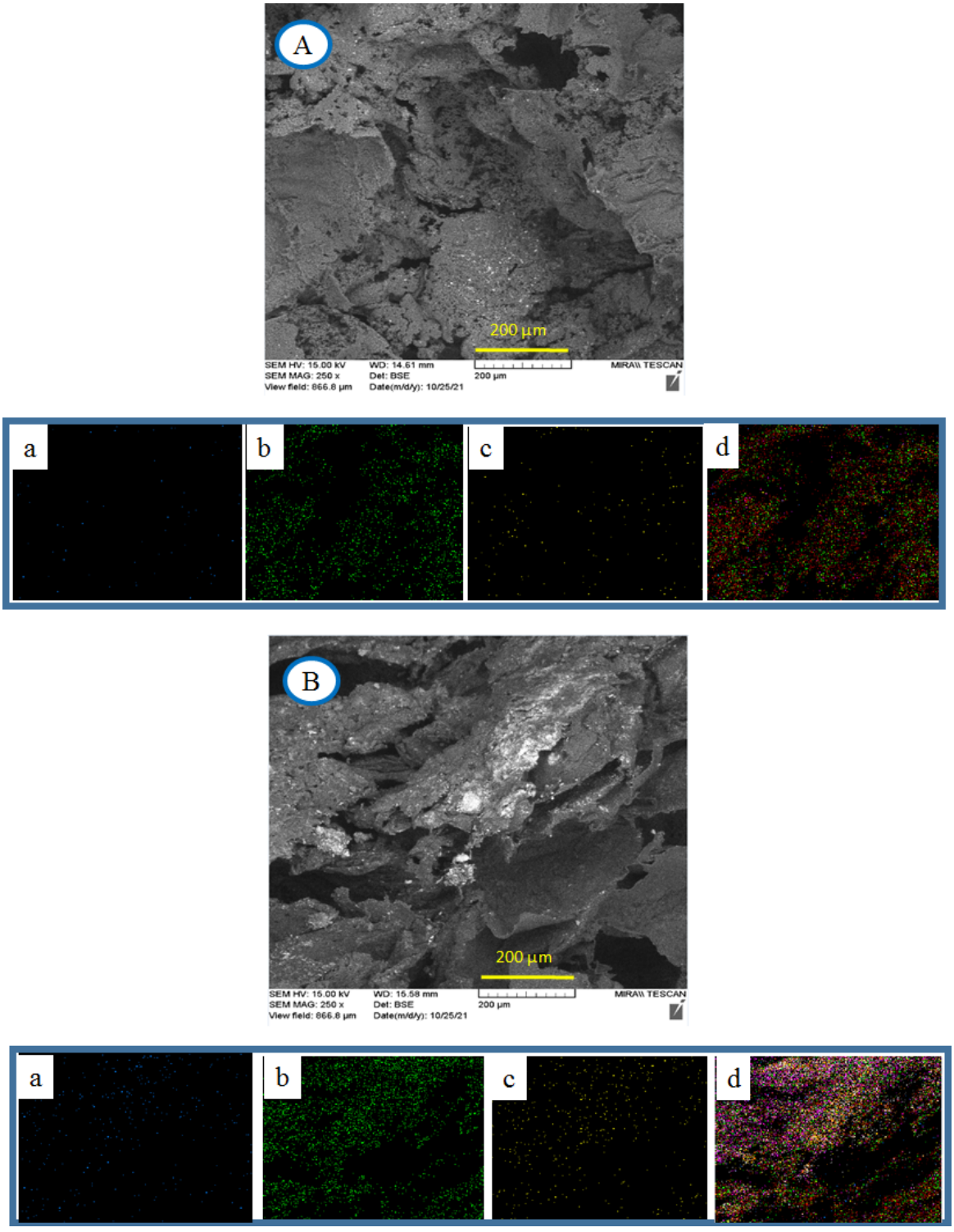

Figure 3. SEM/EDX elemental mapping of (A) PGS/PCL/Ch/HA3% and (B) PGS/PCL/Ch/HA5%, showing (A,B) SEM image, (a) calcium (Ca) distribution, (b) oxygen (O) distribution, (c) phosphorus (P) distribution, and (d) combined elemental mapping.

Table 3. EDS elemental analysis results for PGS/PCL/Ch/HA3% and PGS/PCL/Ch/HA5% scaffolds.

Sample	Element (%)			
	Ca	P	O	Ca/P
PGS/PCL/Ch/HA3%	49.1	6.2	17.4	7.9
PGS/PCL/Ch/HA5%	26.3	10.2	15.9	2.5

all other groups ($p < 0.01$). Chitosan, as a naturally hydrophilic polymer, contributes significantly to this property through its polar functional groups, creating an optimal physicochemical environment for cell adhesion and proliferation. This effect is evident in the lower contact angle observed for the PGS/PCL/Ch sample compared to the PGS/PCL scaffold, confirming chitosan's role in improving surface wettability.

While the PGS/PCL scaffold was used as a primary reference for initial comparisons due to its fundamental composition serving as a baseline, complete pairwise comparisons between all sample groups were conducted to thoroughly evaluate the dataset. These comprehensive statistical analyses confirmed that all modifications resulted in significant improvements in hydrophilicity compared to the baseline, while also revealing significant differences between various modified compositions.

The results revealed that n-HA incorporation increases hydrophilicity through polar surface interactions, hydroxyapatite-PGS composites show maximum wettability, and chitosan's inherent hydrophilicity enhances scaffold performance. These results collectively demonstrate how compositional modifications can effectively tune the surface properties of scaffolds to potentially improve their biological performance.

3.1.3 Swelling behavior analysis

Swelling refers to the absorption of liquid molecules by a polymer network, accompanied by the partial dissolution of polymer chains. This property serves as a critical indicator of a scaffold's capacity to support cell adhesion and proliferation. As demonstrated in Fig. 4 B, all composite scaffolds exhibited a substantial increase in PBS absorption over the tested time intervals (0.5, 1, 2, 4, 7, and 24 h). Among these, the PGS/PCL/Ch scaffold displayed the highest swelling percentage, suggesting its superior liquid retention capability (Sani et al., 2021). The absorption profiles of the scaffolds in PBS solution across these time points are systematically presented in Figure 3B, highlighting their differential swelling behaviors.

3.1.4 Hydrolytic degradation

Understanding the degradation mechanisms of biopolymers is crucial for predicting the long-term behavior of biomaterials. PGS degrades rapidly, which is why the hydrophobic polyester PCL is an excellent choice for modulating its degradation rate. Additionally, blending PCL with hydrophilic materials like chitosan and HA nanoparticles can further enhance the degradation rate. As a natural polymer, chitosan improves hydrophilicity, thereby accelerating degradation.

In this study, the hydrolytic degradation of pure PGS, PGS-PCL, PGS-PCL-Ch, and PGS-PCL-Ch-HA scaffolds—containing varying nanoparticle concentrations (3% and 5%)-was evaluated over time intervals of 1, 3, 7, 14, 28, and 40 days (figure 4). The composite scaffolds exhibited weight losses ranging from 0.4% (for pure PGS/PCL) to 42% (for PGS/PCL/Ch). Surprisingly, scaffolds with higher HA nanoparticle content did not show the anticipated increase in degradation rate, possibly due to differences in water absorption properties (Rostamian et al., 2020; Sani et al., 2021). As seen in figure 5, PGS/PCL/Ch and PGS/PCL/Ch/HA scaffolds experienced the most significant weight loss. While a higher HA content was expected to accelerate degradation, the results did not support this hypothesis, likely because of variations in water uptake behavior (Sani et al., 2021).

3.1.5 Mechanical properties of scaffolds

Cartilage serves as a resilient biological hydrogel that distributes mechanical loads across articulating surfaces while minimizing wear in diarthrodial joints. Assessing the mechanical properties of scaffolds is essential to ensure structural stability and suitability for tissue engineering applications, as these properties directly influence ECM regeneration (Erdal et al., 2020; Zhang et al., 2017).

In this study, the mechanical behavior of composite scaffolds, including compressive strength and elongation at break, was evaluated (Fig. 6 A, and B). Dry scaffold testing revealed that HA nanoparticles enhanced the mechanical properties of PGS/PCL/Ch composites. Specifically,

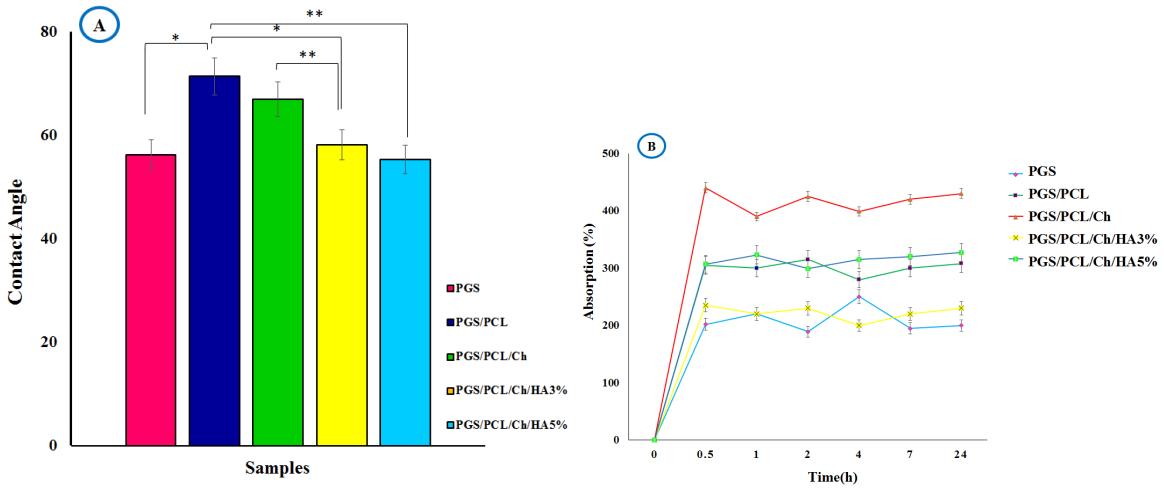

Figure 4. The key hydrophilicity and swelling characteristics of the scaffolds. (A) Displays the contact angle measurements, which were used to evaluate surface wettability. (B) Illustrates the PBS absorption capacity of the scaffolds after 24 h, demonstrating their swelling behavior.

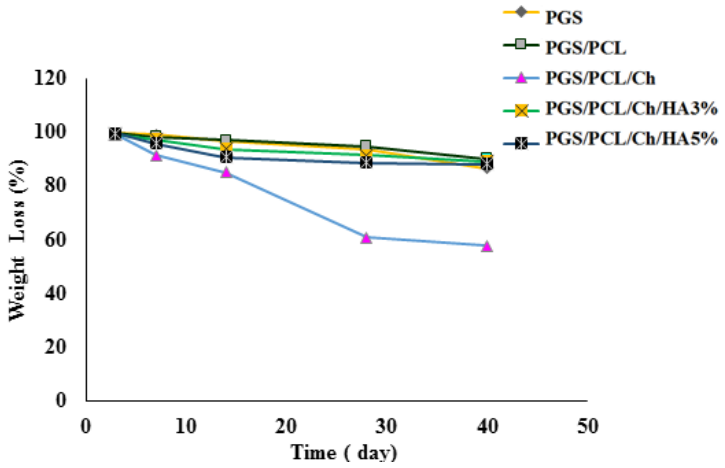

Figure 5. Hydrolytic degradation behavior of the samples over time in PBS.

compressive strength increased with higher HA nanoparticle content, showing a significant correlation between the two. The PGS/PCL/Ch/HA 5% scaffold demonstrated a 25% higher compressive strength compared to PGS/PCL/Ch and a 40% increase compared to pure PGS under dry conditions. However, in wet conditions, the compressive strength of PGS/PCL/Ch/HA 5% scaffolds decreased compared to PGS/PCL/Ch/HA 3%, likely due to increased swelling. Specifically, the compressive strength of PGS/PCL/Ch/HA 5% was 15% lower than PGS/PCL/Ch/HA 3% in wet conditions. No significant differences ($p > 0.05$) were observed among PGS, PGS/PCL, and PGS/PCL/Ch scaffolds in terms of compressive strength.

Elongation at break ranged from 70.08% (PGS/PCL/Ch/HA 5%) to 83.06% (pure PGS). This represents an 18.5% decrease in maximum elongation between pure PGS and PGS/PCL/Ch/HA 5% scaffolds. In dry conditions, elongation decreased upon adding PCL to PGS but increased with higher HA nanoparticle content. The incorporation of 5% HA into PGS/PCL/Ch resulted in a 12% increase in elongation compared to PGS/PCL/Ch without HA. Notably, incorporating 5% HA into the PGS/PCL/Ch matrix significantly improved elongation ($p < 0.05$), consistent with prior studies on HA-reinforced polymers (Asgharnejad-Laskoukalayeh et al., 2022). However, in wet conditions, elongation changes among PGS, PGS/PCL, PGS/PCL/Ch, and PGS/PCL/Ch/HA 5% scaffolds were not statistically significant ($p > 0.05$).

Interestingly, adding 3% HA nanoparticles led to a significant reduction in elongation ($p < 0.01$). The PGS/PCL/Ch/HA 3% scaffold showed a 22% lower elongation value compared to PGS/PCL/Ch under dry conditions.

3.1.6 Thermal degradation of scaffolds

Figure 7 presents the TGA thermograms of the samples, heated at a rate of 10 °C/min up to 600 °C. Thermal degradation occurred between 240-470 °C for all scaffolds. PGS/PCL-based samples exhibited lower thermal stability than pure PGS due to PCL's inferior heat resistance. However, the incorporation of chitosan and HA nanopar-

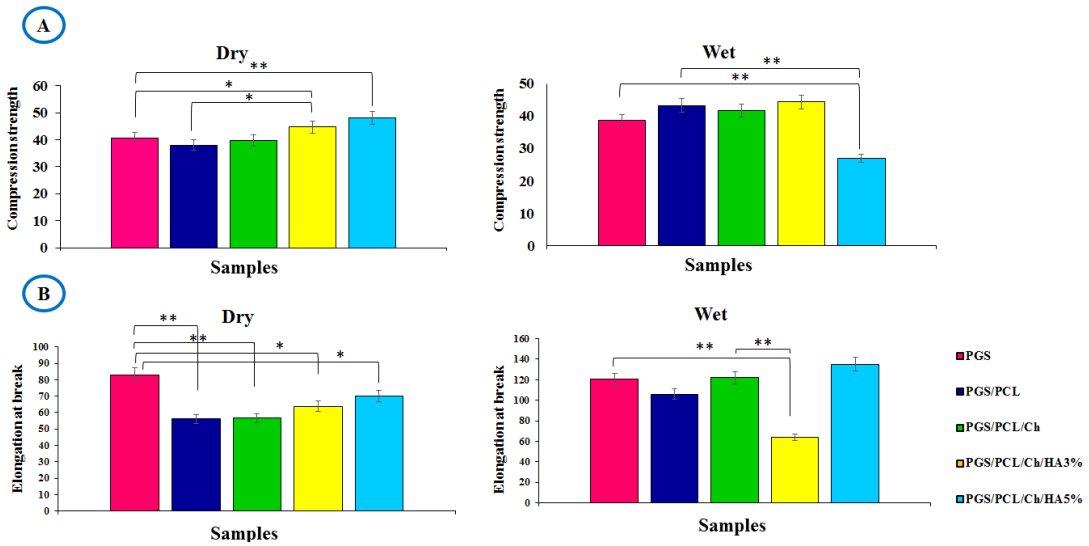

Figure 6. Mechanical characterization of scaffolds: (A) compressive strength and (B) elongation at break under dry and wet conditions. Data represent mean values ± SEM (n = 3); *$p < 0.05$, **$p < 0.01$ indicate statistical significance.

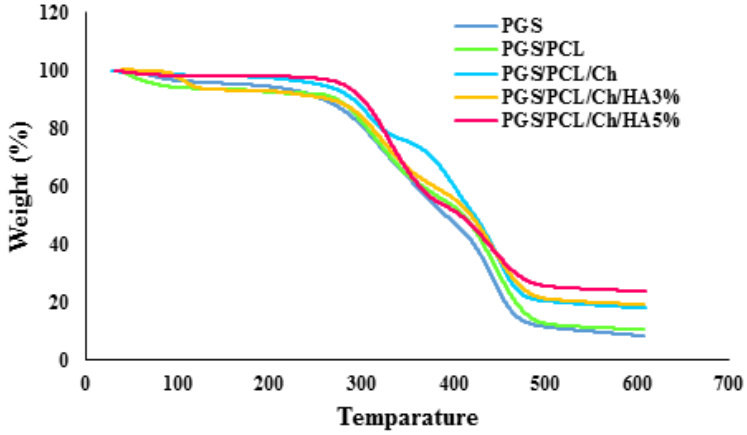

Figure 7. Thermogravimetric analysis (TGA) curves of PGS, PGS/PCL, PGS/PCL/Ch, and PGS/PCL/Ch/HA scaffolds, showing thermal degradation profiles from 30-600 °C at a heating rate of 10°C/min under nitrogen atmosphere.

ticles partially compensated for this instability, delaying degradation compared to PGS/PCL alone (Rostamian et al., 2020). The addition of chitosan-a natural biopolymer with a higher degradation temperature—shifted the onset of thermal decomposition to higher temperatures in PGS/PCL/Ch composites. These scaffolds displayed two-stage weight loss, first stage (190–320 °C) dehydration of chitosan rings and the second stage (330–480 °C) degradation of PGS ester linkages.

Hydroxyapatite nanoparticles, stable up to 600 °C, further enhanced thermal stability in nanocomposites (3% and 5% HA). Well-dispersed HA acted as an insulating barrier, improving heat resistance. This effect likely stems from electrostatic and hydrogen bonding between polar groups in PGS/PCL/Ch and Ca^{2+} ions and hydroxyl groups in HA (Rosenbalm et al., 2016).

3.1.7 Crystallinity of scaffolds

The crystallinity of PGS-based materials was analyzed using X-ray diffraction (XRD), as shown in figure 8 A. The XRD pattern of pure PGS pre-polymer exhibited two peaks at $2\theta = 19.5°$ and 21.3°, corresponding to the (110) and (200) planes of semi-crystalline PGS, respectively, confirming its partial crystallinity. While typically amorphous, PGS can become semi-crystalline depending on its synthesis conditions, including time, temperature, and pressure (Rejali et al., 2024). Since, PCL is also a semi- crystalline polymer, with two main peaks at $2\theta = 21.3°$ and $2\theta = 23.7°$, assigned to the (110) and (200) planes (JCPDS No. 00-060-0518) (Fakhrali et al., 2021), the PGS/PCL composite

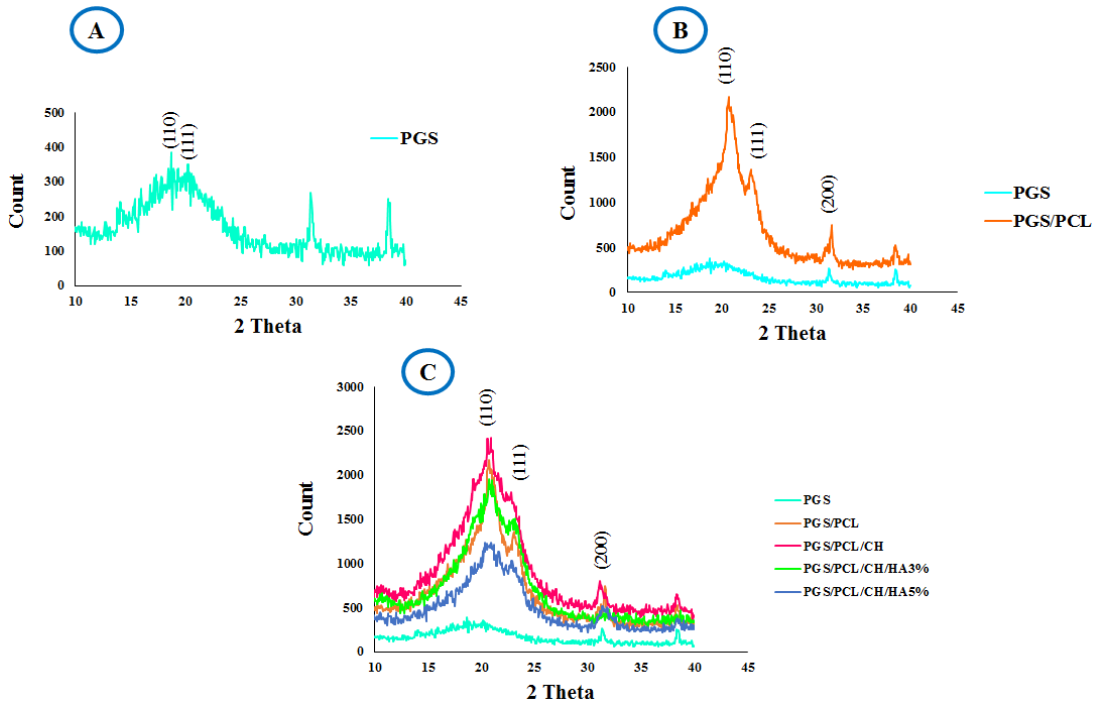

Figure 8. X-ray diffraction patterns of (A) pure PGS, (B) PGS/PCL composite, and (C) PGS/PCL/Ch with varying HA nanoparticle content (3% and 5%), demonstrating crystallinity changes in the scaffold materials.

(Fig. 8B) displayed sharper peaks at $2\theta = 21.3°$, 23.7°, and 32° (Fakhrali et al., 2021; Silva et al., 2020), indicating enhanced crystallinity compared to pure PGS and PCL. This increase in crystallinity is attributed to the semi-crystalline structure of PCL (Barbato et al., 2001; Erdal et al., 2020). The peaks at $2\theta = 19.5°$ and 21.3°correspond to PGS, confirming the presence of both polymers in the composite (Asgharnejad-Laskoukalayeh et al., 2022). The PGS/PCL/Ch scaffold (Fig. 8 C) exhibited even sharper diffraction peaks, suggesting improved crystallization and structural stability. However, the addition of hydroxyapatite (HA) nanoparticles introduced additional diffraction peaks at $2\theta = 25.9°$, 31.7°, 32.9°, 34.1°, and 39.8°, which are indexed to the (200), (211), (112), (300), and (310) planes of HA (JCPDS No. 09-0432). These characteristic peaks confirm the presence of crystalline HA within the polymer matrix. The overall crystallinity slightly decreased, likely due to strong diffraction from nanohydroxyapatite crystals and electrostatic interactions between Ca^{2+}in nHA and polar groups in the composite matrix, which altered the material's structural organization (Asgharnejad-Laskoukalayeh et al., 2022; Nasari et al., 2023).

3.1.8 Scaffold chemical structure

Fourier transform infrared spectroscopy (FTIR) was used to characterize the chemical structure of PGS-based scaffolds. The FTIR spectrum of PGS prepolymer, synthesized from a 1:1 molar ratio of sebacic acid and glycerol, exhibited characteristic absorption bands including a broad hydroxyl stretching vibration at 3426 cm^{-1}, alkane CH_2 stretching vibrations at 2928 cm^{-1} and 2856 cm^{-1}, and ester-related C=O and C-O stretching vibrations at 1734 cm^{-1} and 1094 cm^{-1} respectively, confirming successful polymerization as reported in previous studies (figure 9). FTIR analysis of PCL revealed characteristic absorption bands at: 1732 cm^{-1} (carbonyl stretching vibration), 1160 cm^{-1} (ester C-O-C stretching), and 2839-2977 cm^{-1} (aliphatic CH_2 symmetric/asymmetric stretches). Additional peaks at 1293 cm^{-1} (C-C stretching) and 1238 cm^{-1} (asymmetric C-O-C stretching) were also observed (Asgharnejad-Laskoukalayeh et al., 2022; Nasari et al., 2023). The PGS/PCL composite spectrum contained all characteristic peaks from both polymers, verifying their coexistence. Incorporation of chitosan introduced new absorptions at 1097 cm^{-1} (C-O stretch) and 1570 cm^{-1} (amide II band), the latter indicating chemical interaction between PGS carboxyl groups and chitosan amine groups (Asgharnejad-Laskoukalayeh et al., 2022). For hydroxyapatite-containing composites (3% and 5% HA), additional vibrational bands appeared in the 500-1000 cm^{-1} region corresponding to phosphate groups, with specific HA peaks at 620 $cm^{-1}$and 800 cm^{-1} confirming its presence. The hydroxyl stretching band at 3400 cm^{-1} showed reduced intensity due to hydrogen bonding between chitosan amine groups and HA hydroxyl groups. These FTIR results collectively demonstrate the successful incorporation of all constituent materials (PGS, PCL, Chitosan, and HA) in each nanocomposite formulation (Asgharnejad-Laskoukalayeh et al., 2022; Nasari et al., 2023).

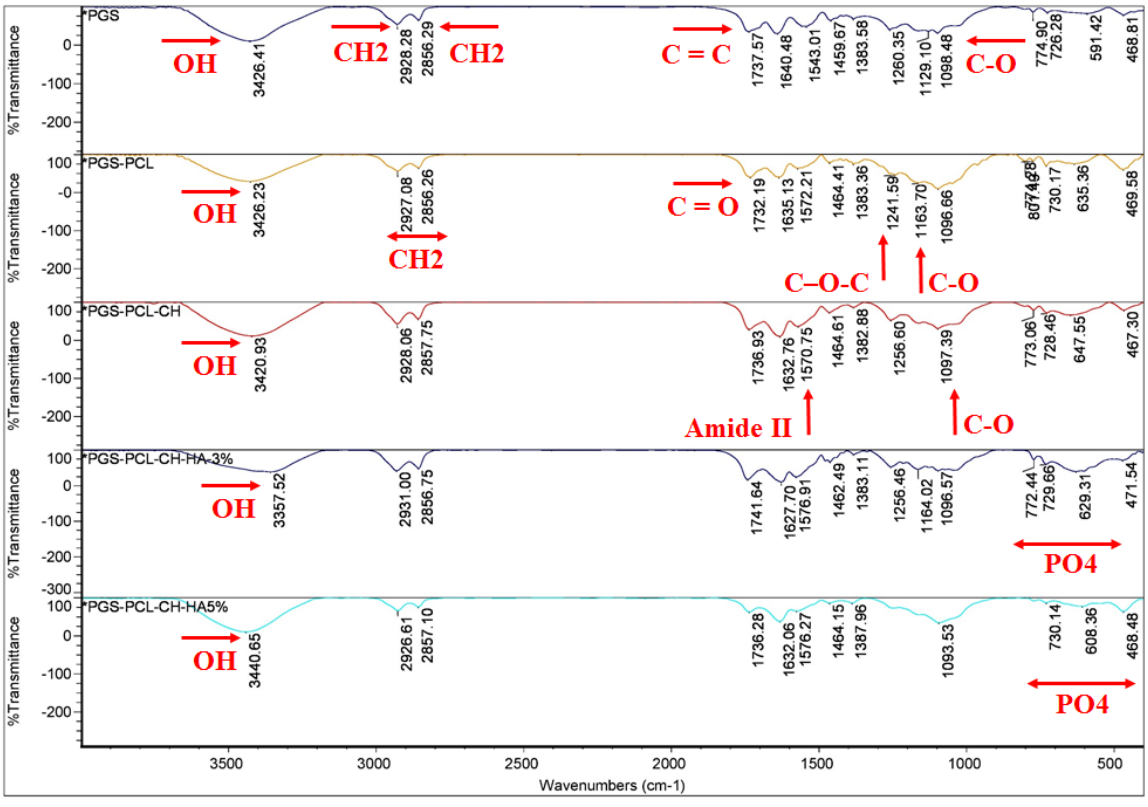

Figure 9. FTIR spectra of pure PGS, PGS/PCL blend, PGS/PCL/Ch composite, and PGS/PCL/Ch scaffolds containing 3% and 5% hydroxyapatite nanoparticles, respectively, showing characteristic functional group vibrations.

3.2 Cellular characterization

3.2.1 Cell viability and cell attachment

The biocompatibility of PGS, PGS/PCL, PGS/PCL/Ch, PGS/PCL/Ch/HA3%, and PGS/PCL/Ch/HA5% scaffolds was evaluated by assessing cell proliferation and attachment over 1, 7, and 14 days (figure 10). Initial observations revealed that PGS/PCL scaffolds initially exhibited inhibitory effects on cell growth, consistent with previous reports, though cell proliferation increased after 24 h compared to the control group (Asgharnejad-Laskoukalayeh et al., 2022). Statistical comparisons between all groups at day 1 showed no significant differences in initial cell attachment ($p > 0.05$ for all pairwise comparisons).

By day 7, a significant enhancement in cell growth was observed for PGS/PCL/Ch and PGS/PCL/Ch/HA (3% and 5%) scaffolds relative to both pure PGS and PGS/PCL groups ($p < 0.05$), with PGS/PCL/Ch/HA5% showing approximately 45% higher viability than pure PGS and 32% higher than PGS/PCL. Furthermore, the PGS/PCL/Ch/HA5% scaffold showed significantly higher cell viability compared to the PGS/PCL/Ch group ($p < 0.05$), demonstrating an 18% increase.

Notably, after 14 days, PGS/PCL/Ch/HA3% and PGS/PCL/Ch/HA5% scaffolds demonstrated superior cell viability compared to other formulations (Asgharnejad-Laskoukalayeh et al., 2022; Nasari et al., 2023), showing approximately twice the cell viability of pure PGS and PGS/PCL scaffolds (2.1-fold and 2.0-fold increase, respectively) with statistically significant differences observed in all relevant pairwise comparisons ($p < 0.01$ for comparisons with PGS, PGS/PCL, and PGS/PCL/Ch groups). The PGS/PCL/Ch/HA5% scaffold also showed 1.5-fold higher cell viability compared to PGS/PCL/Ch scaffolds. No significant difference was found between the PGS/PCL/Ch/HA3% and PGS/PCL/Ch/HA5% groups ($p > 0.05$). This improved performance can be attributed to chitosan's natural hydrophilicity and biocompatibility, facilitated by its amine and hydroxyl functional groups that promote MSC attachment. Furthermore, the incorporation of hydroxyapatite nanoparticles enhanced the overall biocompatibility of the PGS/PCL matrix (Talouki et al., 2023; Yi et al., 2018). As shown in figure 10, all nanocomposite scaffolds exhibited enhanced cell viability and biocompatibility after 14 days in culture. These results confirm that PGS/PCL/Ch and PGS/PCL/Ch/HA scaffolds (3% and 5% HA) provide a more favorable microenvironment for sustained cell proliferation, aligning with findings from previous studies (Asgharnejad-Laskoukalayeh et al., 2022; Guo et al., 2014; Yi et al., 2018).

SEM analysis was performed after 3 days of cell culture to examine cellular interactions with various scaffold surfaces, including PGS, PGS/PCL, PGS/PCL/Ch, and PGS/PCL/Ch/HA (3% and 5%) composites (figure 11). The images revealed enhanced cell-scaffold interactions in PGS/PCL/Ch/HA formulations, particularly with both 3% and 5% HA concentrations. This improved adhesion can be attributed to the presence of polar functional groups on hydroxyapatite nanoparticles, which enhance surface hydrophilicity a critical factor for cellular attachment (Guo et al., 2014; Yi et al., 2018). Similarly, PGS/PCL/Ch scaffolds demonstrated favorable cell adhesion properties due to chitosan's inherent hydrophilicity. Furthermore, the in-

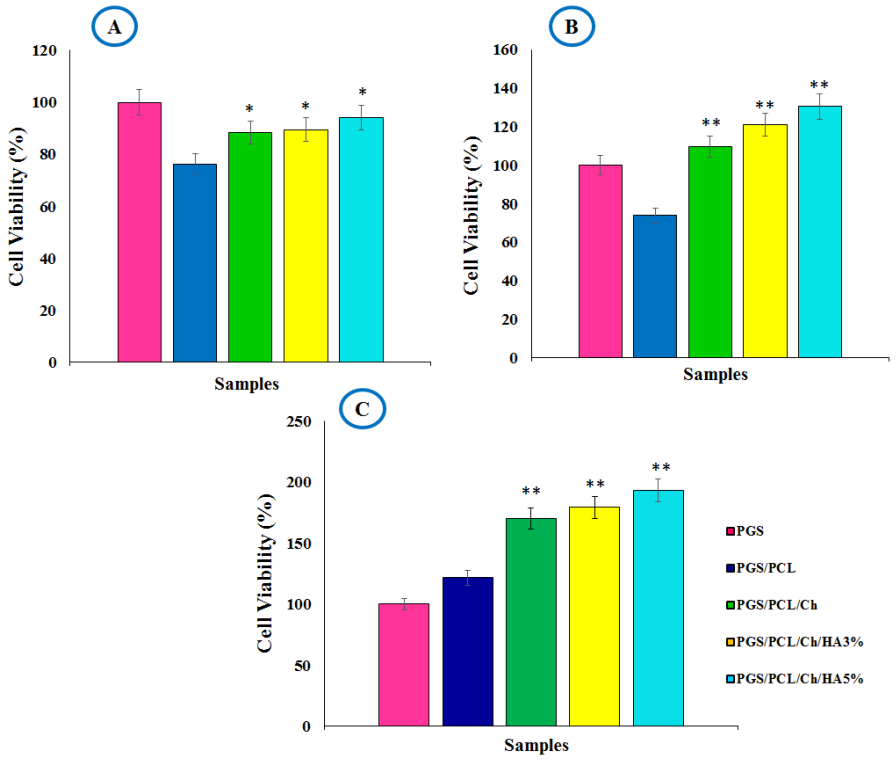

Figure 10. *In vitro* assessment of hMSC viability and proliferation on scaffold materials at (A) 1 day, (B) 7 days, and (C) 14 days post-seeding. Data represent mean ± SEM (n = 3) with statistical significance (*$p < 0.05$, **$p < 0.01$) versus control cells.

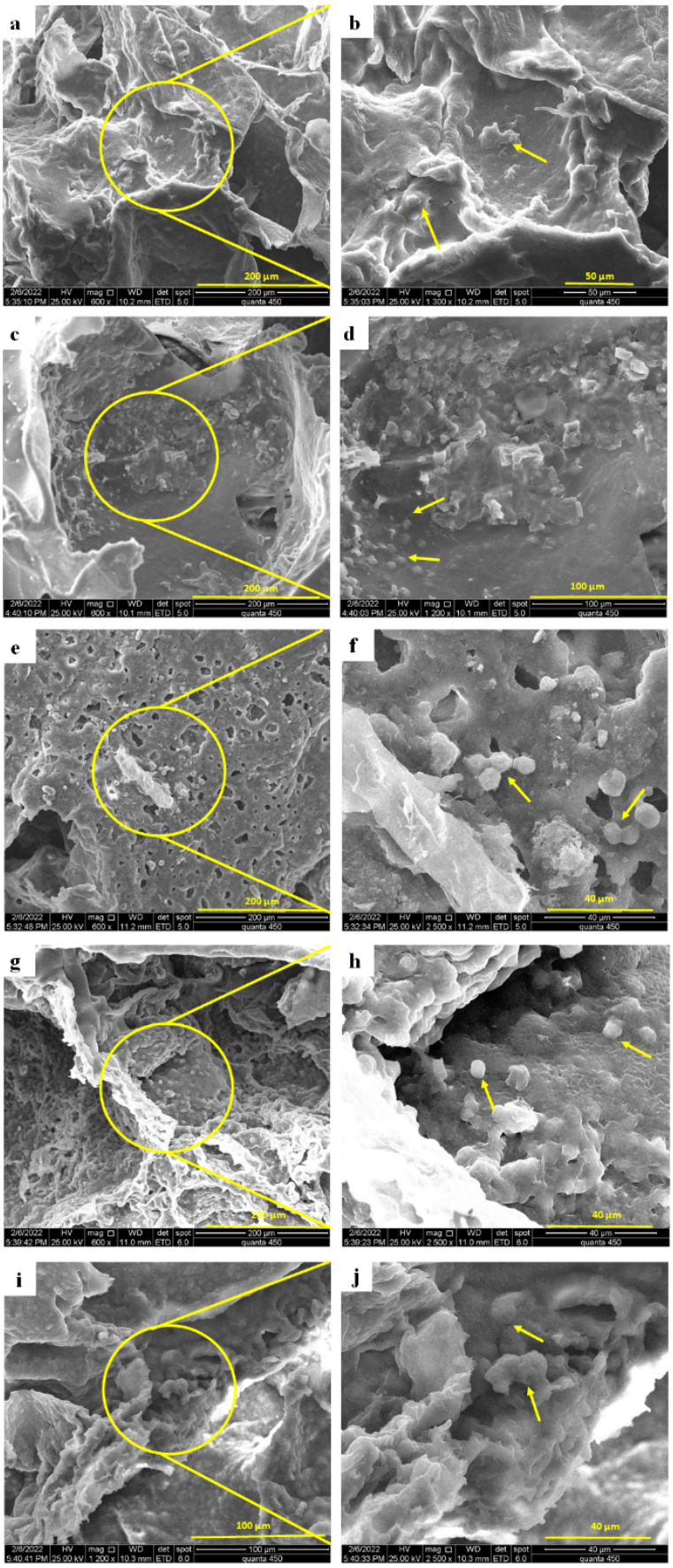

Figure 11. Scanning electron micrographs of adipose-derived mesenchymal stem cells cultured for 3 days on (a, b) PGS, (c, d) PGS/PCL, (e, f) PGS/PCL/Ch, (g, h) PGS/PCL/Ch/HA3%, and (i, j) PGS/PCL/Ch/HA5% scaffolds, demonstrating cell morphology and adhesion characteristics.

corporation of n-HA promoted greater cell proliferation during the 3-day culture period, owing to its natural biocompatibility and the presence of surface hydroxyl and Ca^{2+} groups (Asgharnejad-Laskoukalayeh et al., 2022). These findings collectively demonstrate that n-HA significantly enhances the composite's cellular compatibility and adhesive properties.

3.2.2 Cell differentiation

The chondrogenic potential of the scaffolds was assessed through evaluation of cartilage-specific gene expression (COL2A1, ACAN, and SOX9) and extracellular matrix deposition after 21 days of cell culture (figures 12). Quantitative analysis revealed significantly enhanced expression of COL2A1, ACAN, and SOX9 transcription factor in scaffolds containing 3% and 5% nHA compared to other formulations (Fig. 12 A). The primary effect of nHA incorporation was a significant enhancement in chondrogenic gene expression, with expression levels in both PGS/PCL/Ch/HA3% and PGS/PCL/Ch/HA5% groups being significantly higher than in the PGS, PGS/PCL, and PGS/PCL/Ch groups ($p < 0.01$ for all comparisons), approximately 2.5-3.2 times higher than in pure PGS scaffolds and 1.8-2.3 times higher than in PGS/PCL/Ch scaffolds. No statistically significant difference was observed between the 3% and 5% nHA groups for any gene ($p > 0.05$). This marked up-regulation of chondrogenic markers demonstrates the critical role of nHA in promoting cartilage differentiation, consistent with previous reports (Asgharnejad-Laskoukalayeh et al., 2022). The observed gene expression patterns align with established chondrogenic differentiation pathways, where SOX9 serves as the master regulator of COL2A1, ACAN, and COMP expression during mesenchymal stem cell commitment to the chondrocyte lineage (Wang et al., 2003). Complementary histological evaluation through Alcian blue staining confirmed these findings, with PGS/PCL/Ch/HA scaffolds (3% and 5%) exhibiting significantly greater glycosaminoglycan (GAG) deposition compared to control groups after 21 days (Fig. 12 B, C). This pro-chondrogenic effect of nHA was further confirmed through enhanced matrix production, with both HA-containing scaffolds having significantly higher GAG levels than all other groups ($p < 0.01$ vs. PGS, PGS/PCL, and PGS/PCL/Ch). The GAG deposition in PGS/PCL/Ch/HA5% scaffolds was approximately 3.1 times higher than in pure PGS and 1.9 times higher than in PGS/PCL/Ch scaffolds, while the PGS/PCL/Ch group also showed significantly higher GAG deposition than the pure PGS and PGS/PCL groups ($p < 0.05$). This enhanced matrix production likely stems from the com-

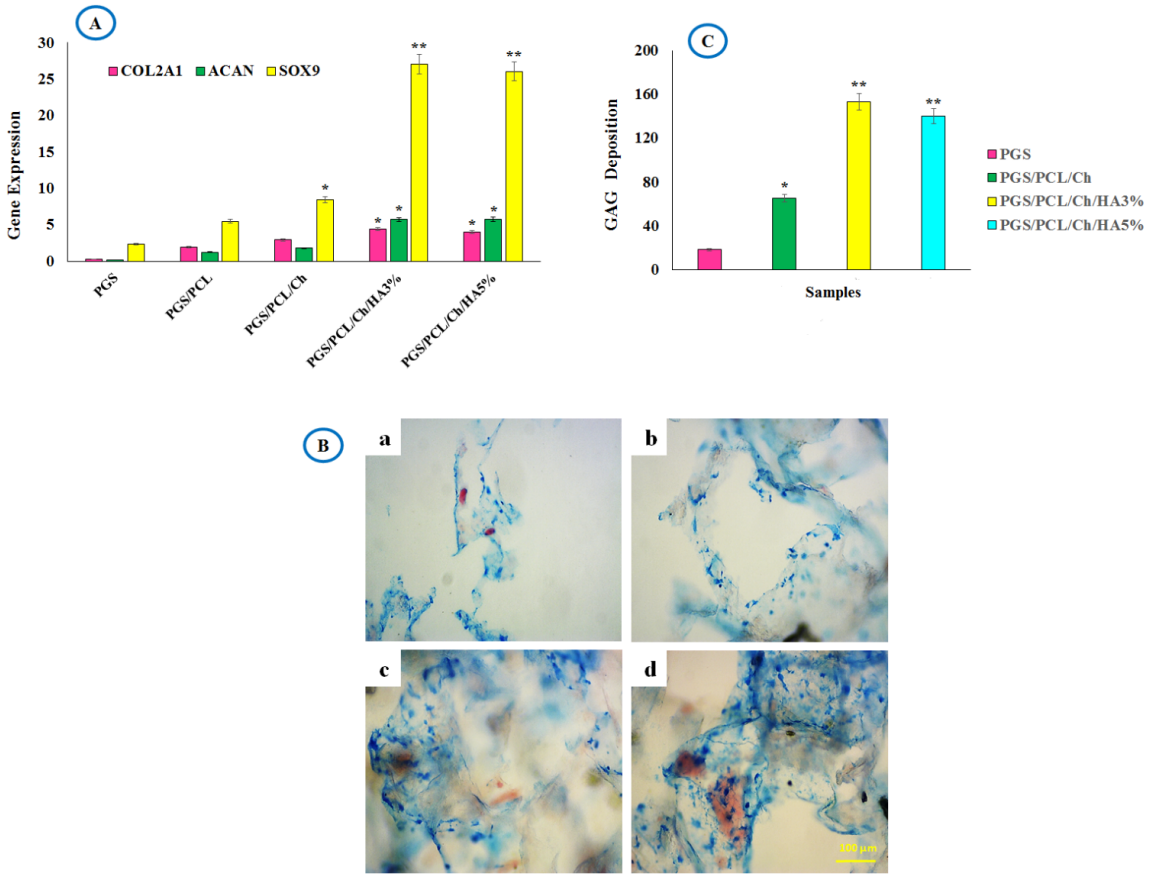

Figure 12. Chondrogenic differentiation and glycosaminoglycan (GAG) deposition in cells cultured on PGS-based scaffolds. (A) Relative mRNA expression of chondrogenic markers (COL2A1, ACAN, SOX9) after 21-day culture on PGS, PGS/PCL/Ch, and PGS/PCL/Ch/HA scaffolds, demonstrating significantly enhanced chondrogenic differentiation in HA-containing composites ($p < 0.05$). (B) Representative histological images of Alcian blue-stained scaffolds after 21 days: (a) PGS, (b) PGS/PCL/Ch, and (c-d) PGS/PCL/Ch/HA (3% and 5%), revealing increased proteoglycan deposition (blue) in HA-incorporated groups. Scale bar: 100 µm. (C) Quantitative analysis of GAG content normalized to DNA, confirming higher matrix deposition in PGS/PCL/Ch/HA scaffolds compared to controls ($p < 0.01$). Data presented as mean ± SD ($n = 3$).

bined effects of (1) The inherent hydrophilicity of chitosan and hydroxyapatite, (2) Their capacity to retain proteoglycans, and (3) Their structural mimicry of native cartilage extracellular matrix (Engelmayr Jr et al., 2008).
The superior performance of HA-containing scaffolds in both gene expression and matrix deposition assays underscores their potential for cartilage tissue engineering applications. These results collectively demonstrate that the incorporation of hydroxyapatite nanoparticles into PGS-based scaffolds creates a microenvironment particularly conducive to chondrogenic differentiation and cartilage-like tissue formation.

4. Discussion

Poly(glycerol sebacate) (PGS) has demonstrated excellent potential for tissue engineering applications due to its favorable mechanical properties, high plasticity, ease of processing, and good biocompatibility (Liu et al., 2016). Its versatility has been shown in various applications including nerve, cartilage, skin, bone, and cardiac tissue engineering (Gaharwar et al., 2014; Sant et al., 2013). However, certain limitations such as low mechanical strength, poor hydrophilicity, and rapid surface erosion degradation have necessitated the development of strategies to enhance its properties (Aghajan et al., 2020; Chen et al., 2011; JS et al., 2000). Our approach of blending PGS with other polymers and fillers has successfully addressed these challenges, as evidenced by the improved mechanical stability, hydrophilicity, and controlled degradation rate of our composite scaffolds. This strategy aligns with previous work by Rostamian et al. who demonstrated that PGS-co-PCL scaffolds exhibit tunable properties suitable for soft tissue engineering applications (Horkay and Basser, 2020), and by Gaharwar et al. who showed that covalent crosslinks between carbon nanotubes and PGS significantly enhance mechanical properties (Ye et al., 2018).
The incorporation of natural and synthetic polymers with hydroxyapatite nanoparticles in our scaffold design builds upon several established findings in the field. Aghajan et al. previously developed a PGS-based nanocomposite incorporating gelatin, graphene oxide, and clay nanoparticles through in situ polymerization (Aghajan et al., 2020), while Chen et al. demonstrated that halloysite nanotubes could effectively modify PGS's physical properties and degradation rate (Chen et al., 2011). Our results confirm and extend these findings, showing that the addition of PCL and HA nanoparticles leads to significant improvements in mechanical properties, hydrophilicity, and degradation profile. When compared to the SA/NC/HA composite scaffolds developed by Shahbazi et al., which achieved excellent tensile (10.5 MPa) and compressive (0.99 MPa) moduli, our PGS/PCL/Chitosan/HA system provides a critically advanced biological characterization. While their work established a strong mechanical foundation suitable for cartilage, it lacked comprehensive validation of chondrogenic differentiation, an area where our scaffolds demonstrate significant upregulation of key genes (Collagen II, Aggrecan, Sox9) and effective suppression of osteogenic fate (Osteocalcin). Zhao et al. similarly demonstrated that the incorporation of silica glass particles enhanced both the mechanical characteristics and surface wettability of PGS-based hybrid materials (Zhao et al., 2015), and by Lau et al. who showed that β-tricalcium phosphate incorporation improved hydrophilicity, degradation rate, and cell viability in PGS scaffolds (Lau et al., 2020).
The chondrogenic potential of our composite scaffolds is supported by extensive literature demonstrating the benefits of combining synthetic and natural polymers with hydroxyapatite nanoparticles for cartilage tissue engineering. Chitosan, renowned for its biocompatibility, antibacterial (Ke et al., 2021; Nelson and Rosowsky, 2002), anti-inflammatory, antifungal, and anticancer properties (Amirani et al., 2020; Aranaz et al., 2021; Shih et al., 2019), holds immense potential in cartilage tissue engineering due to its cationic nature enabling controlled drug release, hydrophilicity for conforming to irregular lesion shapes (Guillén-Carvajal et al., 2023; Kim et al., 2023), wound-healing carrier capabilities (Ueno et al., 2001), tissue-mimetic physicochemical properties (Deptuła et al., 2023), and viscoelastic hydrogels that transfer mechanical loads to chondrocytes-promoting their survival and guiding chondrogenic differentiation (Li et al., 2019). Our findings align with studies by Wise et al. (Wise et al., 2009) and Ousema et al. (Ousema et al., 2012) who demonstrated that PCL scaffolds can enhance chondrogenic marker expression in MSCs, as well as with work by Huang et al. (Huang et al., 2021) who showed that HA-containing scaffolds support chondrocyte proliferation and phenotype maintenance. The enhanced chondrogenic differentiation observed in our study, characterized by increased expression of collagen II, aggrecan, and Sox9 genes, mirrors results reported by Spadaccio et al. in PLLA/HA nanocomposites (Spadaccio et al., 2009) and by Calabrese et al. in gelatin/HAP hybrids (Calabrese et al., 2017).
The structural and functional characteristics of our scaffolds meet critical requirements for cartilage regeneration. The porous architecture, confirmed by SEM imaging, facilitates nutrient transport and cell infiltration, while the tunable degradation rate matches the timeline of extracellular matrix regeneration. Mechanical testing revealed that PCL incorporation enhances strength while HA nanoparticles further improve performance, although we observed that higher HA concentrations (5%) may compromise wet-state mechanical properties. This finding is consistent with the work of Talouki et al. (Talouki et al., 2023), who reported a remarkable decrease in the wet-state compressive strength of PGS/PCL/Gel/HA scaffolds at 5% HA concentration. Our study directly addresses this challenge by identifying and optimizing for a 3% HA concentration, which maintains mechanical integrity in a physiological environment while providing enhanced biological performance. These findings build upon previous work demonstrating the importance of balanced composition in tissue engineering scaffolds (Zheng et al., 2014). The successful cell adhesion, proliferation, and chondrogenic differentiation observed in our study, particularly in PGS/PCL/Ch/HA scaffolds, confirms their potential for cartilage repair applications while avoiding undesired osteogenic differentiation, as evidenced by suppressed osteocalcin expression (Nham, 2019; Pullig et al.,

2000; Yi et al., 2018).

Our investigation reveals that the surface properties of PGS/PCL/Ch/HA scaffolds successfully replicate key aspects of the low-friction interface characteristic of native articular cartilage. The composite scaffolds exhibit markedly enhanced hydrophilicity (Section 3.1.2), facilitating the formation of a stable boundary lubrication layer through improved water retention. This hydrophilic character is further reinforced by the exceptional swelling capacity of the PGS/PCL/Ch formulation (Section 3.1.3), ensuring sustained hydration under physiological conditions. Simultaneously, SEM analysis (Section 3.1.3) demonstrates uniformly smooth surface topography with homogeneous nHA distribution, effectively minimizing direct contact and mechanical interlocking.

However, these friction-reducing characteristics are constrained by inherent material limitations. The enhanced hydrophilicity achieves an optimal balance with mechanical integrity, as evidenced by the compromised wet-state properties observed at higher nHA concentrations (Section 3.1.5). Furthermore, the degradation profile (Section 3.1.8) indicates temporal limitations in maintaining the boundary lubrication layer. The concentration-dependent bioactivity of nHA also reaches a saturation point, as demonstrated by the comparable chondrogenic performance between 3% and 5% nHA groups (Section 3.2.2).

While direct tribological quantification remains for future investigation, the current findings establish a robust foundation for low-friction performance through synergistic surface optimization. Subsequent research will focus on quantitative friction measurements while addressing these identified constraints through advanced material strategies that balance lubricating functionality with structural durability. This comprehensive evaluation of scaffold properties and biological performance, which includes direct comparisons with contemporary studies, clearly distinguishes the achievements of our work. We have not only developed a scaffold with competitive mechanical and biological properties but have also provided a more optimized and balanced solution for cartilage regeneration compared to the seminal works of Shahbazi et al. and Yousefi Talouki et al., particularly in overcoming the wet-state mechanical limitations and delivering comprehensive chondrogenic evidence. This advances our understanding of composite biomaterials for cartilage tissue engineering and provides a foundation for future clinical translation.

5. Conclusion

This study successfully developed an innovative composite scaffold system based on PGS reinforced with PCL, chitosan, and hydroxyapatite nanoparticles (nHA) for cartilage tissue engineering. The systematic investigation revealed that nHA concentration serves as a decisive factor in directing chondrogenic differentiation of human adipose-derived mesenchymal stem cells. The optimized scaffold containing 5% nHA demonstrated exceptional performance across multiple parameters, achieving a compressive strength of 1.8 MPa under wet conditions that approaches native cartilage mechanical properties, while maintaining excellent cell viability of 82.3%. Most notably, this formulation induced a remarkable 3.2-fold upregulation of cartilage-specific markers and enhanced glycosaminoglycan deposition by 58% compared to control groups, confirming its potent chondrogenic capacity.

The strategic material design leveraged the unique advantages of each component: PGS provided essential elastomeric properties, PCL contributed structural integrity, chitosan enhanced hydrophilicity and cellular interactions, while nHA delivered crucial bioactive signals. This synergistic combination successfully created a biomimetic microenvironment that mimicked native cartilage extracellular matrix, promoting robust cell-matrix interactions and supporting sustained chondrogenesis without exogenous growth factors.

These findings establish the PGS/PCL/Ch/nHA composite as a promising platform for cartilage regeneration therapies. The demonstrated composition-dependent bioactivity, combined with tunable physical properties, offers significant potential for clinical translation. Future work will focus on preclinical validation in established animal models and optimization of structural parameters to enhance nutrient diffusion and tissue integration, ultimately advancing toward clinical application in cartilage repair and regeneration.

Ethical Approval

This study was based on the use of ADMSCs acquired from the Iranian Biologi cal Resource Center. None of experiments involved the use of animals or clinical subjects.

Authors contributions

P.Y.: Conceptualization, Investigation, Methodology, Visualization, Resources, Writing original draft.
R.T.: Investigation, Methodology, Visualization, Writing original draft, Review & editing.
S.S.: Supervision, Project administration, Validation, Review & editing.
S.Z.: Investigation, Project administration, Writing – review & editing.
S.H.: Visualization, Validation, Review & editing.
S.M. S: Review & editing, Validation, Visualization.
M.H.N: Validation, Review & editing.
V. G: Project administration, Data curation, Writing – review & editing.
The author(s) read and approved the final manuscript.

Availability of data and materials

The raw/processed data required to reproduce these findings are available on request from the corresponding author. The data are not publicly available at this time as the data also forms part of an ongoing study.

Conflict of interests

The authors declare that they have no known competing financial interests or personal relationships that could have appeared to influence the work reported in this paper.

References

Aghajan M. H., Panahi-Sarmad M., Alikarami N., Shojaei S., Saeidi A., Khonakdar H. A., Shahrousvan M., Goodarzi V. (2020) Using solvent-free approach for preparing innovative biopolymer nanocomposites based on PGS/gelatin. *European Polymer Journal* 131:109720.

Aleksander-Konert E., Paduszyński P., Zajdel A., Dzierżewicz Z., Wilczok A. (2016) In vitro chondrogenesis of Wharton's jelly mesenchymal stem cells in hyaluronic acid-based hydrogels. *Cellular & Molecular Biology Letters* 21:1–13.

Amirani E., Hallajzadeh J., Asemi Z., Mansournia M. A., Yousefi B. (2020) Effects of chitosan and oligochitosans on the phosphatidylinositol 3-kinase-AKT pathway in cancer therapy. *International Journal of Biological Macromolecules* 164:456–467.

Aranaz I., Alcántara A. R., Civera M. C., Arias C., Elorza B., Heras Caballero A., Acosta N. (2021) Chitosan: An overview of its properties and applications. *Polymers* 13 (19): 3256.

Asgharnejad-Laskoukalayeh M., Golbaten-Mofrad H., Jafari S. H., Seyfikar S., Yousefi Talouki P., Jafari A., Goodarzi V., Zamanlui S. (2022) Preparation and characterization of a new sustainable bio-based elastomer nanocomposites containing poly (glycerol sebacate citrate)/chitosan/n-hydroxyapatite for promising tissue engineering applications. *Journal of Biomaterials Science, Polymer Edition* 33:2385–2405.

Baji A., Wong S.-C., Srivatsan T., Njus G. O., Mathur G. (2006) Processing methodologies for polycaprolactone-hydroxyapatite composites: a review. *Materials and Manufacturing Processes* 21 (2): 211–218.

Balakrishnan B., Banerjee R. (2011) Biopolymer-based hydrogels for cartilage tissue engineering. *Chemical Reviews* 111 (8): 4453–4474.

Barbato F., La Rotonda M. I., Maglio G., Palumbo R., Quaglia F. (2001) Biodegradable microspheres of novel segmented poly (ether-ester-amide) s based on poly (ε-caprolactone) for the delivery of bioactive compounds. *Biomaterials* 22:1371–1378.

Biondi M., Ungaro F., Quaglia F., Netti P. A. (2008) Controlled drug delivery in tissue engineering. *Advanced Drug Delivery Reviews* 60 (2): 229–242.

Calabrese G., Forte S., Gulino R., Cefalì F., Figallo E., Salvatorelli L., Maniscalchi E. T., Angelico G., Parenti R., Gulisano M. (2017) Combination of collagen-based scaffold and bioactive factors induces adipose-derived mesenchymal stem cells chondrogenic differentiation *in vitro*. *Frontiers in Physiology* 8:50.

Chen Q.-Z., Liang S.-L., Wang J., Simon G. P. (2011) Manipulation of mechanical compliance of elastomeric PGS by incorporation of halloysite nanotubes for soft tissue engineering applications. *Journal of the Mechanical Behavior of Biomedical Materials* 4 (8): 1805–1818.

Deptuła M., Zawrzykraj M., Sawicka J., Banach-Kopeć A., Tylingo R., Pikuła M. (2023) Application of 3D-printed hydrogels in wound healing and regenerative medicine. *Biomedicine & Pharmacotherapy* 167:115416.

Dorotka R., Bindreiter U., Macfelda K., Windberger U., Nehrer S. (2005) Marrow stimulation and chondrocyte transplantation using a collagen matrix for cartilage repair. *Osteoarthritis and Cartilage* 13 (8): 655–664.

Engelmayr Jr G. C., Cheng M., Bettinger C. J., Borenstein J. T., Langer R., Freed L. E. (2008) Accordion-like honeycombs for tissue engineering of cardiac anisotropy. *Nature Materials* 7:1003–1010.

Epp J. (2016) X-ray diffraction (XRD) techniques for materials characterization. In Materials characterization using nondestructive evaluation (NDE) methods. Elsevier:81–124.

Erdal N. B., Lando G. A., Yadav A., Srivastava R. K., Hakkarainen M. (2020) Hydrolytic degradation of porous crosslinked poly (ε-caprolactone) synthesized by high internal phase emulsion templating. *Polymers* 12:1849.

Eshraghi S., Das S. (2012) Micromechanical finite-element modeling and experimental characterization of the compressive mechanical properties of polycaprolactone–hydroxyapatite composite scaffolds prepared by selective laser sintering for bone tissue engineering. *Acta Biomaterialia* 8 (8): 3138–3143.

Fakhrali A., Nasari M., Poursharifi N., Semnani H. D.a nd Salehi, Ghane M., Mohammadi S. (2021) Biocompatible graphene-embedded PCL/PGS-based nanofibrous scaffolds: a potential application for cardiac tissue regeneration. *Journal of Applied Polymer Science* 138:51177.

Farjaminejad S., Shojaei S., Goodarzi V., Khonakdar H. A., Abdouss M. (2021) Tuning properties of bio-rubbers and its nanocomposites with addition of succinic acid and ε-caprolactone monomers to poly (glycerol sebacic acid) as main platform for application in tissue engineering. *European Polymer Journal* 159:110711.

Gaharwar A. K., Nikkhah M., Sant S., Khademhosseini A. (2014) Anisotropic poly (glycerol sebacate)-poly (ε-caprolactone) electrospun fibers promote endothelial cell guidance. *Biofabrication* 7 (1): 015001.

Garcia C. E. G., Lardy B., Bossard F., Martínez F. A. S., Rinaudo M. (2021) Chitosan based biomaterials for cartilage tissue engineering: Chondrocyte adhesion and proliferation. *Food Hydrocolloids for Health* 1:100018.

Ge Z., Li C., Heng B. C., Cao G., Yang Z. (2012) Functional biomaterials for cartilage regeneration. *Journal of biomedical materials research Part A* 100 (9): 2526–2536.

Gellynck K., Verdonk P. C., Van Nimmen E., Almqvist K. F., Gheysens T., Schoukens G., Van Langenhove L., Kiekens P., Mertens J., Verbruggen G. (2008) Silkworm and spider silk scaffolds for chondrocyte support. *Journal of Materials Science: Materials in Medicine* 19 (11): 3399–3409.

Guillén-Carvajal K., Valdez-Salas B., Beltrán-Partida E., Salomón-Carlos J., Cheng N. (2023) Chitosan, gelatin, and collagen hydrogels for bone regeneration. *Polymers* 15 (13): 2762.

Guo X. L., Lu X. L., Dong D. L., Sun Z. J. (2014) Characterization and optimization of glycerol/sebacate ratio in poly (glycerol-sebacate) elastomer for cell culture application. *Journal of Biomedical Materials Research Part A* 102:3903–3907.

Horkay F., Basser P. J. (2020) Composite hydrogel model of cartilage predicts its load-bearing ability. *Scientific Reports* 10:8103.

Hu M.-Y., Nukavarapu S. (2019) Scaffolds for cartilage tissue engineering. *Handbook of tissue engineering scaffolds: Volume one.,* 211–244.

Huang J., Huang Z., Liang Y., Yuan W., Bian L., Duan L., Rong Z., Xiong J., Wang D., Xia J. (2021) 3D printed gelatin/hydroxyapatite scaffolds for stem cell chondrogenic differentiation and articular cartilage repair. *Biomaterials Science* 9 (7): 2620–2630.

Jelodari S., Ebrahimi Sadrabadi A., Zarei F., Jahangir S., Azami M., Sheykhhasan M., Hosseini S. (2022) New insights into cartilage tissue engineering: improvement of tissue-scaffold integration to enhance cartilage regeneration. *BioMed Research International* 2022 (1): 7638245.

JS S. R. H. S. S., AM D. S. M. D. M., JP K. B. S. F. V., JE Jr M. (2000) Early *in vivo* experience with tissue-engineered trileaflet heart valves. *Circulation* 102 (19 Suppl 3)

Ke C.-L., Deng F.-S., Chuang C.-Y., Lin C.-H. (2021) Antimicrobial actions and applications of chitosan. *Polymers* 13 (6): 904.

Kim Y., Zharkinbekov Z., Raziyeva K., Tabyldiyeva L., Berikova K., Zhumagul D., Temirkhanova K., Saparov A. (2023) Chitosan-based biomaterials for tissue regeneration. *Pharmaceutics* 15 (3): 807.

Kumar B. S., Isloor A. M., Kumar G. M., Inamuddin, Asiri A. M. (2019) Nanohydroxyapatite reinforced chitosan composite hydrogel with tunable mechanical and biological properties for cartilage regeneration. *Scientific Reports* 9 (1): 15957.

Lau C., Al Qaysi M., Owji N., Bayazit M., Xie J., Knowles J., Tang J. (2020) Advanced biocomposites of poly (glycerol sebacate) and β-tricalcium phosphate by in situ microwave synthesis for bioapplication. *Materials Today Advances* 5:100023.

Li J., Chen G., Xu X., Abdou P., Jiang Q., Shi D., Gu Z. (2019) Advances of injectable hydrogel-based scaffolds for cartilage regeneration. *Regenerative Biomaterials* 6 (3): 129–140.

Liu T., Mu H., Shen Z., Song Z., Chen X., Wang Y. (2016) Autologous adipose tissue-derived mesenchymal stem cells are involved in rat liver regeneration following repeat partial hepatectomy. *Molecular Medicine Reports* 13 (3): 2053–2059.

Liu Y., Shah K. M., Luo J. (2021) Strategies for articular cartilage repair and regeneration. *Frontiers in Bioengineering and Biotechnology* 9:770655.

Mad Jin R., Sultana N., Baba S., Hamdan S., Ismail A. F. (2015) Porous PCL/chitosan and nHA/PCL/chitosan scaffolds for tissue engineering applications: fabrication and evaluation. *Journal of Nanomaterials* 2015 (1): 357372.

Nasari M., Poursharifi N., Fakhrali A., Banitaba S. N., Mohammadi S., Semnani D. (2023) Fabrication of novel PCL/PGS fibrous scaffold containing HA and GO through simultaneous electrospinning-electrospray technique. *International Journal of Polymeric Materials and Polymeric Biomaterials* 72:1529–1545.

Nelson R. G., Rosowsky A. (2002) Dicyclic and tricyclic diaminopyrimidine derivatives as potent inhibitors of cryptosporidium parvum dihydrofolate reductase: structure-activity and structure-selectivity correlations. *Antimicrobial Agents and Chemotherapy* 46 (3): 940.

Neves S. C., Teixeira L. S. M., Moroni L., Reis R. L., Van Blitterswijk C. A., Alves N. M., Karperien M., Mano J. F. (2011) Chitosan/Poly (ε-caprolactone) blend scaffolds for cartilage repair. *Biomaterials* 32 (9): 1068–1079.

Nham G. T. H. (2019) Expression of type *II* collagen and aggrecan genes is regulated through distinct epigenetic modifications of their multiple enhancer elements

Ousema P. H., Moutos F. T., Estes B. T., Caplan A. I., Lennon D. P., Guilak F., Weinberg J. B. (2012) The inhibition by interleukin 1 of MSC chondrogenesis and the development of biomechanical properties in biomimetic 3D woven PCL scaffolds. *Biomaterials* 33 (35): 8967–8974.

Pullig O., Weseloh G., Ronneberger D.-L., Käkönen S.-M., Swoboda B. (2000) Chondrocyte differentiation in human osteoarthritis: expression of osteocalcin in normal and osteoarthritic cartilage and bone. *Calcified Tissue International* 67 (3): 230–240.

Rai R., Tallawi M., Grigore A., Boccaccini A. R. (2012) Synthesis, properties and biomedical applications of poly (glycerol sebacate)(PGS): A review. *Progress in Polymer Science* 37 (8): 1051–1078.

Rejali A., Ebrahimian-Hosseinabadi M., Kharazi A. Z. (2024) Polyglycerol Sebacate/polycaprolactone/reduced graphene oxide composite scaffold for myocardial tissue engineering. *Heliyon* 10 (19)

Rezaei F. S., Khorshidian A., Beram F. M., Derakhshani A., Esmaeili J., Barati A. (2021) 3D printed chitosan/polycaprolactone scaffold for lung tissue engineering: hope to be useful for COVID-19 studies. *RSC Advances* 11 (32): 19508–19520.

Rezk A. I., Kim K.-S., Kim C. S. (2020) Poly (ε-caprolactone)/poly (glycerol sebacate) composite nanofibers incorporating hydroxyapatite nanoparticles and simvastatin for bone tissue regeneration and drug delivery applications. *Polymers* 12 (11): 2667.

Rosenbalm T. N., Teruel M., Day C. S., Donati G. L., Morykwas M., Argenta L., Kuthirummal N., Levi-Polyachenko N. (2016) Structural and mechanical characterization of bioresorbable, elastomeric nanocomposites from poly (glycerol sebacate)/nanohydroxyapatite for tissue transport applications. *Journal of Biomedical Materials Research Part B: Applied Biomaterials* 104:1366–1373.

Rostamian M., Kalaee M. R., Dehkordi S. R., Panahi-Sarmad M., Tirgar M., Goodarzi V. (2020) Design and characterization of poly (glycerol-sebacate)-co-poly (caprolactone)(PGS-co-PCL) and its nanocomposites as novel biomaterials: The promising candidate for soft tissue engineering. *European Polymer Journal* 138:109985.

Sani I. S., Rezaei M., Khoshfetrat A. B., Razzaghi D. (2021) Preparation and characterization of polycaprolactone/chitosan-g-polycaprolactone/hydroxyapatite electrospun nanocomposite scaffolds for bone tissue engineering. *International Journal of Biological Macromolecules* 182:1638–1649.

Sant S., Iyer D., Gaharwar A. K., Patel A., Khademhosseini A. (2013) Effect of biodegradation and de novo matrix synthesis on the mechanical properties of valvular interstitial cell-seeded polyglycerol sebacate–polycaprolactone scaffolds. *Acta Biomaterialia* 9 (4): 5963–5973.

Shahzadi L., Zeeshan R., Yar M., Qasim S. B., Chaudhry A. A., Khan A. F., Muhammad N. (2018) Biocompatibility through cell attachment and cell proliferation studies of nylon 6/chitosan/ha electrospun mats. *Journal of Polymers and the Environment* 26 (5): 2030–2038.

Sharma D., Mathur V. P., Satapathy B. K. (2021) Biodegradable and biocompatible 3D constructs for dental applications: Manufacturing options and perspectives. *Annals of Biomedical Engineering* 49 (9): 2030–2056.

Shi H., Zhou Z., Li W., Fan Y., Li Z., Wei J. (2021) Hydroxyapatite based materials for bone tissue engineering: A brief and comprehensive introduction. *Crystals* 11 (2): 149.

Shih P.-Y., Liao Y.-T., Tseng Y.-K., Deng F.-S., Lin C.-H. (2019) A potential antifungal effect of chitosan against Candida albicans is mediated via the inhibition of SAGA complex component expression and the subsequent alteration of cell surface integrity. *Frontiers in Microbiology* 10:602.

Shoajei S., Tafazzoli-Shahdpour M., Shokrgozar M. A., Haghighipour N. (2014) Alteration of human umbilical vein endothelial cell gene expression in different biomechanical environments. *Cell Biology International* 38 (5): 577–581.

Shojaei S., Nikuei M., Goodarzi V., Hakani M., Khonakdar H., Saeb M. (2019) Disclosing the role of surface and bulk erosion on the viscoelastic behavior of biodegradable poly (ε-caprolactone)/poly (lactic acid)/hydroxyapatite nanocomposites. *Journal of Applied Polymer Science*

Silva J. C., Udangawa R. N., Chen J., Mancinelli C. D., Garrudo F. F., Mikael P. E., Cabral J. M., Ferreira F. C., Linhardt R. J. (2020) Kartogenin-loaded coaxial PGS/PCL aligned nanofibers for cartilage tissue engineering. *Materials Science and Engineering: C* 107:110291.

Solheim E., Hegna J., Øyen J., Harlem T., Strand T. (2013) Results at 10 to 14 years after osteochondral autografting (mosaicplasty) in articular cartilage defects in the knee. *The Knee* 20 (4): 287–290.

Spadaccio C., Rainer A., Trombetta M., Vadalá G., Chello M., Covino E., Denaro V., Toyoda Y., Genovese J. A. (2009) Poly-L-lactic acid/hydroxyapatite electrospun nanocomposites induce chondrogenic differentiation of human MSC. *Annals of Biomedical Engineering* 37 (7): 1376–1389.

Talouki P. Y., Tackallou S. H., Shojaei S., Benisi S. Z., Goodarzi V. (2023) The role of three-dimensional scaffolds based on polyglycerol sebacate/polycaprolactone/gelatin in the presence of Nanohydroxyapatite in promoting chondrogenic differentiation of human adipose-derived mesenchymal stem cells. *Biological Procedures Online* 25 (1): 9.

Tew S., Redman S., Kwan A., Walker E., Khan I., Dowthwaite G., Thomson B., Archer C. W. (2001) Differences in repair responses between immature and mature cartilage. *Clinical Orthopaedics and Related Research* 391:S142–S152.

Ueno H., Mori T., Fujinaga T. (2001) Topical formulations and wound healing applications of chitosan. *Advanced Drug Delivery Reviews* 52 (2): 105–115.

Wang Y., Kim Y. M., Langer R. (2003) *In vivo* degradation characteristics of poly (glycerol sebacate). *Journal of Biomedical Materials Research Part A: An Official Journal of The Society for Biomaterials, The Japanese Society for Biomaterials, and The Australian Society for Biomaterials and the Korean Society for Biomaterials* 66:192–197.

Wise J. K., Yarin A. L., Megaridis C. M., Cho M. (2009) Chondrogenic differentiation of human mesenchymal stem cells on oriented nanofibrous scaffolds: engineering the superficial zone of articular cartilage. *Tissue Engineering Part A* 15 (4): 913–921.

Ye H., Zhang K., Kai D., Li Z., Loh X. J. (2018) Polyester elastomers for soft tissue engineering. *Chemical Society Reviews* 47 (12): 4545–4580.

Yi S. W., Kim H. J., Oh H. J., Shin H., Lee J. S., Park J. S., Park K.-H. (2018) Gene expression profiling of chondrogenic differentiation by dexamethasone-conjugated polyethyleneimine with SOX trio genes in stem cells. *Stem Cell Research & Therapy* 9:341.

Zhang Y., Huang X., Yuan Y. (2017) MicroRNA-410 promotes chondrogenic differentiation of human bone marrow mesenchymal stem cells through down-regulating Wnt3a. *American Journal of Translational Research* 9:136.

Zhao X., Hu D. A., Wu D., He F., Wang H., Huang L., Shi D., Liu Q., Ni N., Pakvasa M. (2021) Applications of biocompatible scaffold materials in stem cell-based cartilage tissue engineering. *Frontiers in Bioengineering and Biotechnology* 9:603444.

Zhao X., Wu Y., Du Y., Chen X., Lei B., Xue Y., Ma P. X. (2015) A highly bioactive and biodegradable poly (glycerol sebacate)–silica glass hybrid elastomer with tailored mechanical properties for bone tissue regeneration. *Journal of Materials Chemistry B* 3:3222–3233.

Zheng R., Duan H., Xue J., Liu Y., Feng B., Zhao S., Zhu Y., Liu Y., He A., Zhang W. (2014) The influence of Gelatin/PCL ratio and 3-D construct shape of electrospun membranes on cartilage regeneration. *Biomaterials* 35 (1): 152–164.